Mfsd2b and Spns2 are essential for maintenance of blood vessels during development and in anaphylactic shock

Thanh Nha Uyen Le, Toan Q Nguyen, Pazhanichamy Kalailingam, Yen Thi Kim Nguyen, Viresh Krishnan Sukumar, Clarissa Kai Hui Tan, Farhana Tukijan, Ludovic Couty, Zafrul Hasan, Ilaria del Gaudio, et al.

Cell Reports

Article

Mfsd2b and *Spns2* are essential for maintenance of blood vessels during development and in anaphylactic shock

Graphical abstract

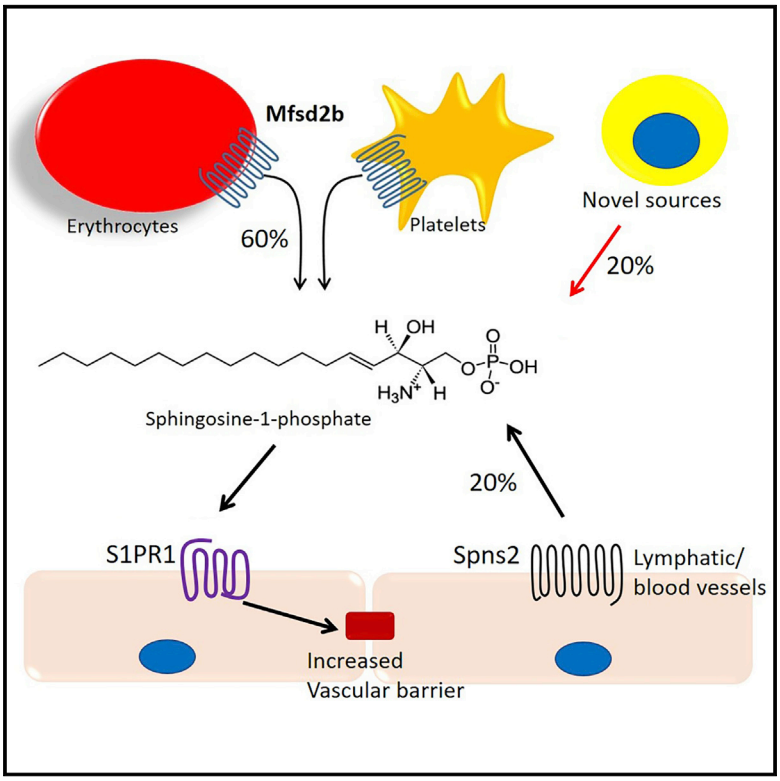

Authors

Thanh Nha Uyen Le, Toan Q. Nguyen, Pazhanichamy Kalailingam, ..., Amaury Cazenave-Gassiot, Eric Camerer, Long N. Nguyen

Correspondence

bchnnl@nus.edu.sg

In brief

Sphingosine-1-phosphate (S1P) is a potent lipid mediator. Using mouse models, Le et al. demonstrate that the sources of extracellular S1P released from Mfsd2b and Spns2 are essential for protection of the vasculature from hemorrhages during development and in anaphylactic shock.

Highlights

- Global deletion of *Mfsd2b* and *Spns2* causes embryonic lethality
- *Mfsd2b* and *Spns2* in Mx1Cre-sensitive cells provide 80% of the plasma S1P
- 20% of the plasma S1P in Mx1Cre-sensitive cells is independent of these transporters
- Plasma S1P is essential for maintenance of vascular integrity and vascular tone

Le et al., 2022, Cell Reports *40*, 111208
August 16, 2022
https://doi.org/10.1016/j.celrep.2022.111208

CellPress

Cell Reports

CellPress
OPEN ACCESS

Article

Mfsd2b and *Spns2* are essential for maintenance of blood vessels during development and in anaphylactic shock

Thanh Nha Uyen Le,[1,8] Toan Q. Nguyen,[1,8] Pazhanichamy Kalailingam,[1] Yen Thi Kim Nguyen,[1] Viresh Krishnan Sukumar,[1] Clarissa Kai Hui Tan,[1] Farhana Tukijan,[1] Ludovic Couty,[2] Zafrul Hasan,[1,7] Ilaria Del Gaudio,[2] Markus R. Wenk,[1,3] Amaury Cazenave-Gassiot,[1,3] Eric Camerer,[2] and Long N. Nguyen[1,3,4,5,6,9,*]

[1]Department of Biochemistry, Yong Loo Lin School of Medicine, National University of Singapore, Singapore 117596, Singapore
[2]Université Paris Cité, PARCC, INSERM U970, 56 Rue Leblanc, 75015 Paris, France
[3]Singapore Lipidomics Incubator (SLING), Life Sciences Institute, National University of Singapore, Singapore 117456, Singapore
[4]Cardiovascular Disease Research (CVD) Program, Yong Loo Lin School of Medicine, National University of Singapore, Singapore 117545, Singapore
[5]Immunology Program, Life Sciences Institute, National University of Singapore, Singapore 117456, Singapore
[6]Immunology Translational Research Program, Yong Loo Lin School of Medicine, National University of Singapore, Singapore 117456, Singapore
[7]Present address: Department of Biochemistry and Molecular Biology, Kumargaon, Sylhet-3114, Shahjalal University of Science and Technology, Bangladesh
[8]These authors contributed equally
[9]Lead contact
*Correspondence: bchnnl@nus.edu.sg
https://doi.org/10.1016/j.celrep.2022.111208

SUMMARY

Sphingosine-1-phosphate (S1P) is a potent lipid mediator that is secreted by several cell types. We recently showed that *Mfsd2b* is an S1P transporter from hematopoietic cells that contributes approximately 50% plasma S1P. Here we report the characterization of compound deletion of *Mfsd2b* and *Spns2*, another S1P transporter active primarily in endothelial cells. Global deletion of *Mfsd2b* and *Spns2* (global double knockout [gDKO]) results in embryonic lethality beyond embryonic day 14.5 (E14.5), with severe hemorrhage accompanied by defects of tight junction proteins, indicating that *Mfsd2b* and *Spns2* provide S1P for signaling, which is essential for blood vessel integrity. Compound postnatal deletion of *Mfsd2b* and *Spns2* using Mx1Cre (ctDKO-Mx1Cre) results in maximal 80% reduction of plasma S1P. ctDKO-Mx1Cre mice exhibit severe susceptibility to anaphylaxis, indicating that S1P from Mfsd2b and Spns2 is indispensable for vascular homeostasis. Our results show that S1P export from *Mfsd2b* and *Spns2* is essential for developing and mature vasculature.

INTRODUCTION

Sphingosine-1-phosphate (S1P) is a potent lipid mediator that is required for lymphocyte egress from lymphoid organs and essential for blood vessel development and function. S1P exerts signaling roles via 5 cognate S1P receptors (S1P1–S1P5). S1P is synthesized from sphingosines by sphingosine kinase 1 (SphK1) and SphK2 (Yanagida and Hla, 2017). Extracellular SphK1 can also generate S1P, but it remains to be determined whether this pathway is physiologically relevant (Venkataraman et al., 2006). S1P is a polar lipid that requires active transport across lipid bilayers. The concentrations of extracellular S1P are tightly regulated to form a gradient with levels ranging from less than 1 nM in interstitial fluid to ~100 nM in lymph and ~1000 nM in the blood (Hla and Dannenberg, 2012; Spiegel and Milstien, 2011; Rosen and Goetzl, 2005). Lymphocytes rely on this gradient of S1P for trafficking. Whether vascular cells are also sensitive to the S1P gradient remains to be established.

An important role of S1P signaling is regulation of lymphocyte trafficking. Mechanistically, S1P binds and stimulates S1P1 on the plasma membrane of lymphocytes to drive their migration from the lymph node parenchyma to the lymphatic circulation. S1P signaling also plays essential roles in the vasculature. Several S1P receptors are expressed in different cell types in blood vessels (Yanagida et al., 2020). Deletion of S1P1 results in embryonic death from embryonic day 12.5 (E12.5) and E14.5 with severe hemorrhage (Liu et al., 2000). Specific ablation of endothelial S1P1 in adult mice also results in impaired vascular integrity (Jung et al., 2012; Gaengel and Betsholtz, 2013; Yanagida et al., 2017). Compound deletion of S1P1 with S1P2 or S1P3 or triple knockout of these receptors results in earlier lethality reminiscent of compound deletion of SphK1 and SphK2 (Kono et al., 2004; Mizugishi et al., 2005), emphasizing that they play non-redundant roles in blood vessels. In line with essential roles of S1P signaling in blood vessels, compound conditional deletion of SphK1 and SphK2 results in vascular leakage and

sensitization to vascular insults (Camerer et al., 2009; Gazit et al., 2016).

To understand how S1P signaling is regulated, it is important to determine which cell types release S1P. By selective deletion of SphK1 and SphK2, it has been established that endothelial and hematopoietic cells are the major sources of plasma S1P (Gazit et al., 2016). In line with these studies, it has been shown that *Spns2* exports S1P from endothelial cells, whereas *Mfsd2b* exports S1P from erythrocytes and platelets (Fukuhara et al., 2012; Vu et al., 2017; Chandrakanthan et al., 2021). Although *Spns2* deletion results in strong lymphopenia, vascular development and function are normal in *Spns2* knockout mice (Mendoza et al., 2012). Global deletion of *Mfsd2b* results in approximately 50% reduction of plasma S1P and renders mice susceptible to passive systemic anaphylaxis (Vu et al., 2017). However, these isolated knockout mice thrive to adulthood, suggesting that *Mfsd2b* and *Spns2* provide redundant sources of S1P to maintain vascular development and homeostasis. To understand the roles of *Mfsd2b* and *Spns2* in S1P export and to address whether additional S1P transporters exist, we performed compound deletion of *Mfsd2b* and *Spns2* before and after birth. Our results show that *Mfsd2b* and *Spns2* together are essential for embryonic development. Lack of both genes resulted in lethality with hemorrhagic phenotypes analogous to S1P1 knockout mice, suggesting that they are essential for S1P delivery to S1P1. We show that *Mfsd2b* and *Spns2* coordinate to provide a major proportion of plasma S1P to maintain homeostasis of the mature vasculature. Our results also suggest that there may be an Mx1-Cre sensitive cell type that delivers S1P to plasma independent of *Mfsd2b* and *Spns2*.

RESULTS

Global deletion of *Mfsd2b* and *Spns2* causes embryonic lethality

We and others have shown recently that *Mfsd2b* and *Spns2* export S1P from the hematopoietic and vascular system, respectively (Fukuhara et al., 2012; Vu et al., 2017; Mendoza et al., 2012). Global deletion of *Mfsd2b* (*Mfsd2b*$^{-/-}$) or *Spns2* (*Spns2*$^{-/-}$) results in incomplete reduction of plasma S1P without overt embryonic phenotypes (Fukuhara et al., 2012; Vu et al., 2017). Single-cell RNA sequencing (RNA-seq) showed that *Mfsd2b* is specifically expressed in primitive and definitive red blood cells (RBCs) (Cao et al., 2019; Figures S1A and S1B). *Spns2* expression is also found in primitive RBCs and endothelial cells (Cao et al., 2019; Figure S1C). To examine whether *Mfsd2b* and *Spns2* are functional during embryonic development, we isolated primitive RBCs and fetal liver cells from the corresponding knockout embryos for transport assays. We showed that primitive RBC from *Mfsd2b*$^{-/-}$ embryos exhibited an approximately 50% reduction of S1P transport activity (Figure 1A). Fetal liver cells from *Mfsd2b*$^{-/-}$ embryos also exhibited slightly reduced S1P transport activity (Figure 1B). Primitive RBCs, but not fetal liver cells from *Spns2*$^{-/-}$ embryos, also had a slight but significant reduction of S1P transport activity (Figures 1C and 1D). These data suggest that *Mfsd2b* and *Spns2* transport functions are active in primitive RBCs during fetal development. To examine whether they are the only physiological S1P transporters, we generated a global knockout of *Mfsd2b* and *Spns2* in mice (*Mfsd2b*$^{-/-}$;*Spns2*$^{-/-}$, hereafter called global double knockout [gDKO]). Expression of both genes was abolished, as confirmed by real-time PCR from fetal liver cells (Figure S2A). Although these male and female breeders carrying a single allele of *Spns2* were healthy and fertile, we observed a small litter size, suggestive of embryonic lethality. We found that gDKO embryos were viable at E12.5 with few obvious defects, although blood vessels in the dorsocaudal regions were slightly dilated (Figure 1E, arrowheads; Figure S2B). However, viable gDKO embryos exhibiting noticeable signs of hemorrhage were found at E13.5 (Figures 1E, arrows, and 1F, arrowhead; Figure S3). We found dead gDKO embryos with signs of severe hemorrhage, especially in the dorsocaudal regions, at E14.5 (Figure 1E, arrows). These results indicate that gDKO embryos die between E13.5 and E14.5 (Table S1). The observed hemorrhagic phenotypes of gDKO embryos are largely reminiscent of S1P1 knockout embryos but slightly less severe than DKO of sphingosine kinases (SphK1/2) (Liu et al., 2000; Mizugishi et al., 2005). Our data show that S1P exported by *Mfsd2b* and *Spns2* is critical for survival and that these are likely the sole S1P transporters active during embryonic development.

Mfsd2b and *Spns2* in Mx1Cre-sensitive cells provide a major fraction of plasma S1P

Previous studies have shown that conditional deletion of SphK1 and SphK2 using Mx1Cre resulted in a greater than 90% S1P reduction in adult mice (Gazit et al., 2016). Mx1Cre drives deletion of floxed genes in hematopoietic cells, endothelial cells, and hepatocytes, suggesting that these cells are the major sources of plasma S1P (Kuhn et al., 1995). To determine whether *Mfsd2b* and *Spns2* mediate export of S1P derived from SphK1 and SphK2 in these cells, we performed compound conditional deletion of *Mfsd2b* and *Spns2* using Mx1Cre (*Mfsd2b*$^{f/f}$;*Spns2*$^{f/f}$;Mx1Cre, hereafter called ctDKO-Mx1Cre). First, to address whether Mx1Cre mediated efficient deletion of *Mfsd2b* and *Spns2* in ctDKO-Mx1Cre mice, we measured S1P transport activity in RBCs and quantified numbers of white blood cells (WBCs), the parameters that are affected by loss of *Mfsd2b* and *Spns2*, respectively. S1P transport activity in RBCs isolated from ctDKO-Mx1Cre was reduced to a similar degree as in RBCs from *Mfsd2b*$^{-/-}$ mice but not in RBCs from *Spns2*$^{-/-}$ mice (Figures 2A and 2B). Expression of *Mfsd2b* protein in RBCs isolated from ctDKO-Mx1Cre mice was also abolished (Figure 2C). Deletion of *Mfsd2b* increases erythrocyte cell volume. This was recapitulated in erythrocytes from ctDKO-Mx1Cre mice (Figure 2D). In line with efficient deletion of *Spns2*, peripheral WBC counts from ctDKO-Mx1Cre mice were as low as in *Spns2*$^{-/-}$ mice (Figure 2E). These data indicate that expression of *Mfsd2b* and *Spns2* was abolished in ctDKO-Mx1Cre mice. Second, we analyzed plasma S1P collected from ctDKO-Mx1Cre mice 1 and 4 months after injection of poly(I:C) (Figure 2F). In these analyses, *Mfsd2b*$^{-/-}$ mice showed an ~55% reduction of plasma S1P, and *Spns2*$^{-/-}$ mice showed an ~12% reduction of plasma S1P (Figures 2G–2I). Plasma S1P levels in

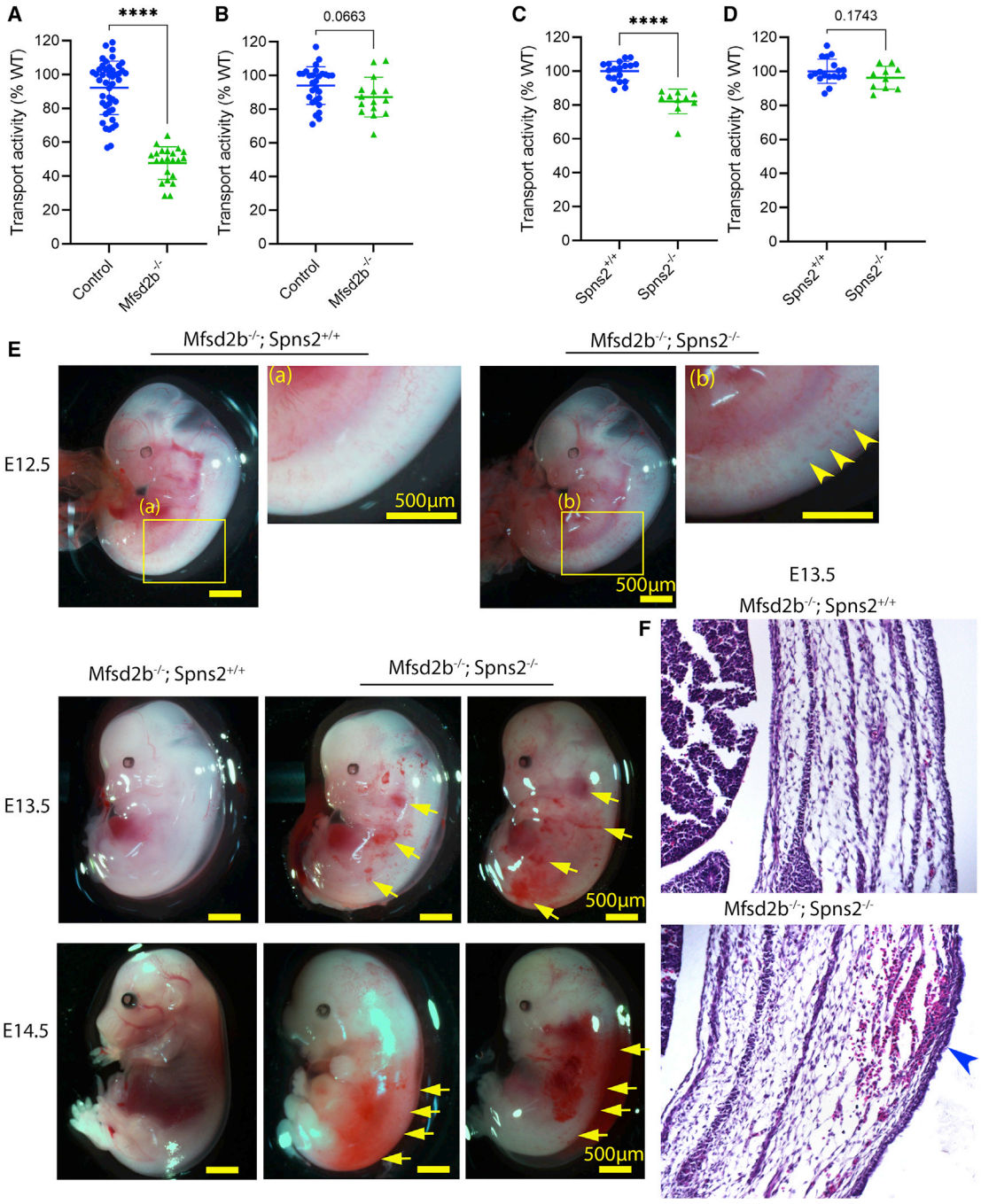

Figure 1. Compound deletion of Mfsd2b and Spns2 causes early embryonic lethality

(A and B) Transport activity of primitive RBCs (A) and fetal liver cells (B) from E17.5–E18.5 *Mfsd2b*$^{-/-}$ and control embryos. ****$p < 0.0001$, t test.

(C and D) Transport activity of primitive RBCs (C) and fetal liver cells (D) from E17.5–E18.5 *Spns2*$^{-/-}$ and WT embryos, respectively. Each symbol represents an embryo. ****$p < 0.0001$, t test.

(E) Deletion of *Mfsd2b* and *Spns2* results in lethality between E13.5 and E14.5. In comparison with *Mfsd2b* knockout embryos carrying native *Spns2* alleles used as controls, embryos with complete loss of the *Mfsd2b* and *Spns2* genes (gDKO) were viable and had normal morphology at E12.5. Blood vessels from lower body parts of gDKO embryos were slightly dilated at E12.5 (top panel, arrowheads) and became prominent at E13.5 (center panel, arrows). Non-viable gDKO embryos with severe hemorrhage were observed at E14.5 (bottom panel, arrows). gDKO embryos died between E13.5 and E14.5. (a) and (b) show enlarged images of lower dorsal regions of control and gDKO embryos.

(F) Representative H&E images of a transverse section of E13.5 control and gDKO embryos. An arrowhead shows the bleeding in the dermis. Images were taken with a 20× objective.

See also Figures S2 and S3 and Table S1.

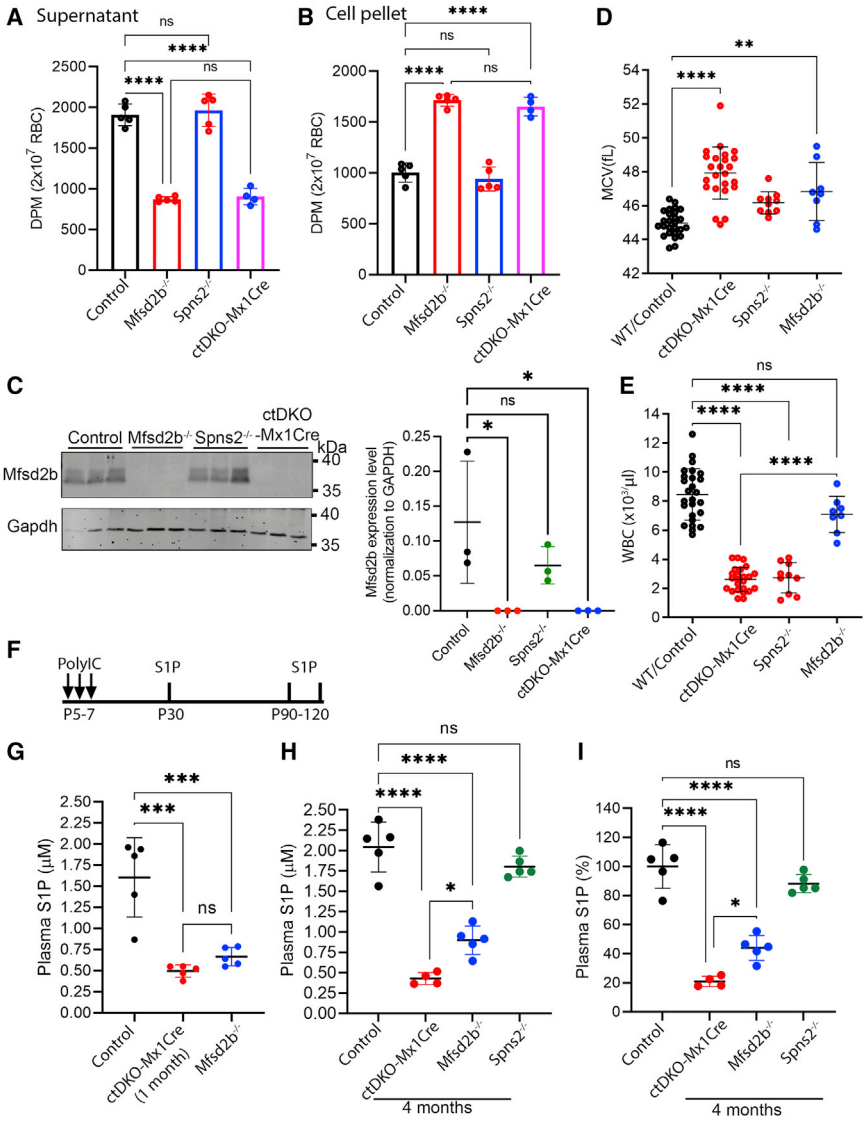

Figure 2. *Mfsd2b* and *Spns2* coordinate to supply a majority of plasma S1P in adult mice

(A and B) Reduced S1P transport activity of erythrocytes from ctDKO-Mx1Cre mice. Shown are supernatant (A) and cell pellet (B) S1P levels from erythrocytes from control, *Mfsd2b*$^{-/-}$, *Spns2*$^{-/-}$, and ctDKO-Mx1Cre mice. The transport activity of erythrocytes from ctDKO-Mx1Cre mice was identical to that of erythrocytes from *Mfsd2b*$^{-/-}$ mice. Data are mean and SD. Each symbol represents one mouse (n = 4–5 per genotype).

(C) Western blot analysis and quantification of Mfsd2b expression in erythrocytes from control, *Mfsd2b*$^{-/-}$, *Spns2*$^{-/-}$, and ctDKO-Mx1Cre mice. Experiments were performed twice (n = 3).

(D) Increased MCV of erythrocytes from ctDKO-Mx1Cre mice.

(E) White blood cell (WBC) counts from WT/control, *Mfsd2b*$^{-/-}$, *Spns2*$^{-/-}$, and ctDKO-Mx1Cre mice.

(F) Deletion strategy of *Mfsd2b* and *Spns2* in ctDKO-Mx1Cre mice induced by poly(I:C) and the time points for S1P analysis.

(G) Plasma S1P level from control, ctDKO-Mx1Cre mice 1 month after poly(I:C) injection and *Mfsd2b*$^{-/-}$ mice. n = 5 per genotype from two experiments. The plasma S1P level from *Mfsd2b*$^{-/-}$ mice is also included for comparison.

(H and I) Concentration (H) and percentage (I) of plasma S1P from 4-month-old control, *Mfsd2b*$^{-/-}$, *Spns2*$^{-/-}$, and ctDKO-Mx1Cre mice. Data are mean ± SD.

****p < 0.0001, ***p < 0.001, **p < 0.01, *p < 0.05; ns, not significant. One-way ANOVA was used.

ctDKO-Mx1Cre mice were decreased by ~70% 1 month after poly(I:C) treatment (Figure 2G) and reduced by ~80% 4 months after poly(I:C) injection (Figures 2H and 2I). These results indicate that *Mfsd2b* and *Spns2* coordinate to contribute to plasma S1P and that Mx1Cre-sensitive cells expressing these two transporters provide approximately 80% of plasma S1P in adult mice. Our results also suggest that more than 10% of plasma S1P may be provided by Mx1Cre-positive cells independent of these two transporters. Based on these results, we selected ctDKO-Mx1Cre mice more than 3 months after poly(I:C) injection with a WBC count lower than 2,500 cells/μL for subsequent experiments.

Embryos lacking *Mfsd2b* and *Spns2* exhibit hemorrhages and cerebral vascular defects

Having demonstrated that *Mfsd2b* and *Spns2* provide essential sources of S1P for development, we examined the causes of lethality of gDKO embryos, focusing on hemorrhage and vascular defects. We stained brain sections of E13.5 embryos with the vascular markers CD31and Glut1 and the RBC marker Ter119. The vascular density in the brain of gDKO appeared to be largely unaffected in the examined regions (Figures 3A and 3B; Figures S4 and S5). However, in addition to peripheral hemorrhage as shown in Figure 1, we found that blood vessels in the central nervous system (CNS) of gDKO embryos at E13.5 were ruptured, with extravasation of RBCs in the ganglionic eminences and hindbrain/hypothalamus (Figures 3A and 3B, arrowheads; Figures S4B and S4C). RBCs were detected in the brain parenchyma, indicating impaired integrity of CNS blood vessels of gDKO (Figures 3A–3C; Figures S4B and S4C). We also found that CNS blood vessels were slightly dilated in the ganglionic eminences but not in the midbrain of gDKO embryos (Figures 3D and 3E). Several blood vessels near the ventricles were severely dilated, a phenotype that is similar to micro-aneurisms (Figures 3A and 3B, arrows). Our results show that deletion of *Mfsd2b* and *Spns2* causes cerebral hemorrhage during embryonic development.

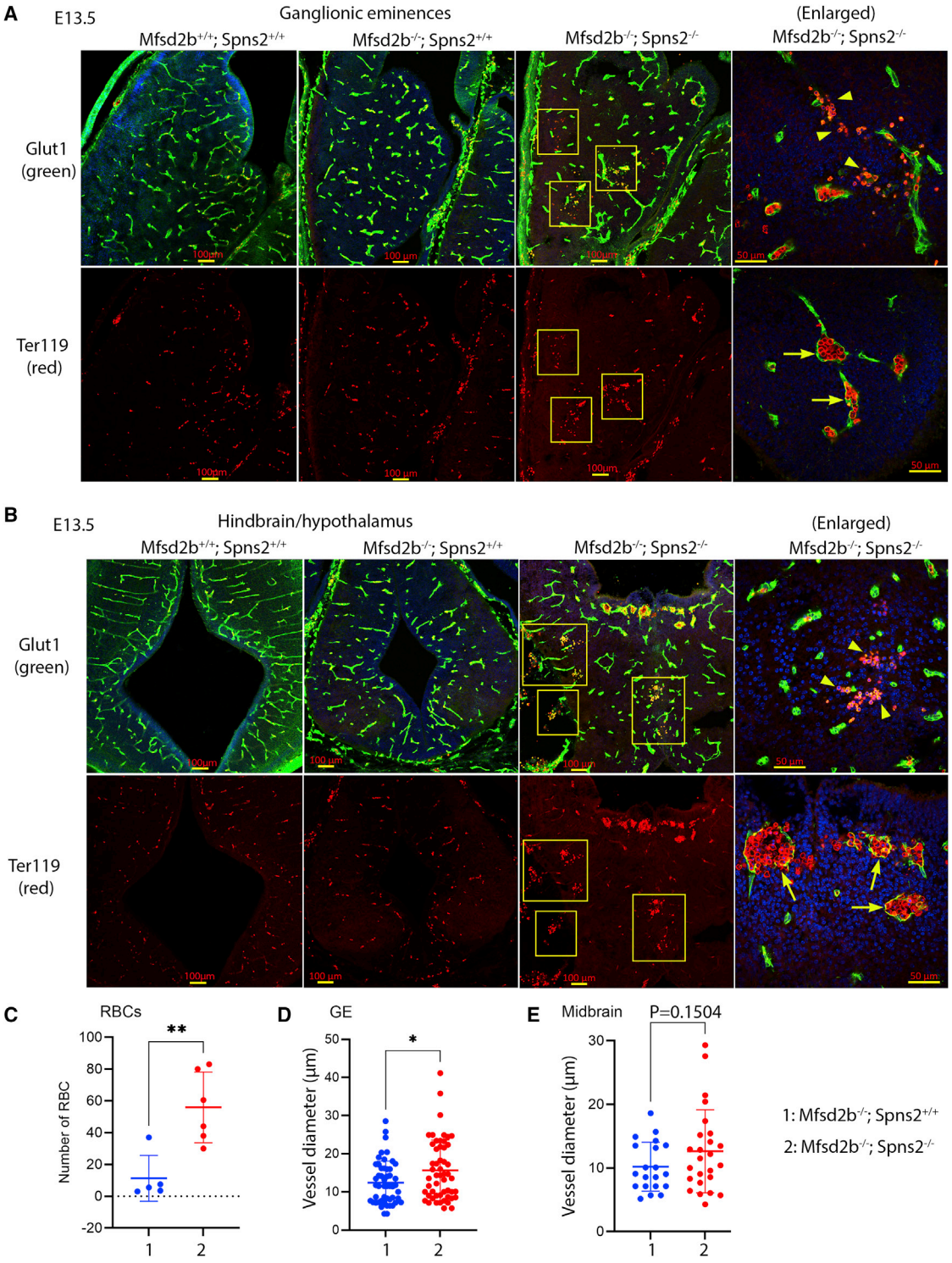

Figure 3. Global deletion of *Mfsd2b* and *Spns2* results in cerebral hemorrhage and vascular defects in embryos

(A) Representative images of ganglionic eminence (GE) regions of WT, *Mfsd2b*$^{-/-}$ (control littermates), and gDKO embryos at E13.5. gDKO embryos displayed hemorrhage, shown by extravasation of RBCs (Ter119 staining) (boxes and arrowheads) and dilated blood vessels (arrows); n = 6 per genotype.

(B) Hemorrhage in hindbrain regions of E13.5 gDKO embryos (boxes indicate hemorrhagic regions). gDKO embryos also exhibited local hemorrhage near ventricular regions (arrowheads). Cerebral blood vessels of E13.5 gDKO fetuses were also dilated (arrows).

(legend continued on next page)

Compound global deletion of *Mfsd2b* and *Spns2* results in cerebral blood vessel rupture

The hemorrhagic phenotypes observed in the brain of gDKO embryos suggest that lack of S1P secretion from *Mfsd2b* and *Spns2* is detrimental to blood vessel integrity in the brain. Loss of pericytes causes hemorrhage in embryos (Lindahl et al., 1997). Thus, we tested whether the coverage of pericytes, the mural cells of CNS blood vessels, is affected in E13.5 gDKO blood vessels. Our results showed that pericyte coverage, shown by PDGFRβ staining, in CNS blood vessels of gDKO embryos was comparable with littermate controls (Figure 4A). Expression of N-cadherin was also unaffected in the brain of gDKO embryos (Figure S6A). Disruption of transforming growth factor β (TGF-β) or canonical WNT signaling pathways results in brain hemorrhage (Stenman et al., 2008; Daneman et al., 2009; Wang et al., 2018; Li et al., 2011; Arnold et al., 2014; Dave et al., 2018; Crist et al., 2019; Hubner et al., 2018). Therefore, we also explored whether expression of phosphorylated Smad4 and β-catenin, the respective components of TGF-β and canonical WNT signaling pathways, is altered. However, both pathways were intact in the brain of gDKO embryos (Figure 4B). Expression of PLVAP, which is upregulated to increase transcytosis in the blood-brain barrier of WNT signaling knockout mice, was comparable between the genotypes (Figures S6B and S6C; Cho et al., 2017; Zhou et al., 2014). These data rule out involvement of TGF-β and canonical WNT signaling in the hemorrhagic phenotypes. Lack of S1P signaling results in compromised expression of adherens and tight junction proteins that may be linked to the fragility of blood vessels in gDKO embryos. We found that the expression pattern of Claudin-5 was disrupted in the hemorrhagic vessels (Figures 4C and 4D, arrowheads; Figure S7A). Quantification of immunostaining signals revealed a significant reduction of Claudin-5 expression (Figure 4E). Expression of VE-cadherin, an adherens junction protein required for maintenance of junctions between endothelial cells, was also reduced in the brain of gDKO embryos (Figures 4D, 4F, and 4G; Figure S7B). S1P signaling is mediated by activation of mitogen-activated protein (MAP) kinases (Jo et al., 2005). We found that lack of *Mfsd2b* and *Spns2* reduced the expression of phosphorylated ERK1/2 (p-ERK1/2), suggestive of low levels of S1P in the brain parenchyma of gDKO embryos (Figures 4H; Figure S7C), whereas expression of the endothelial proteins CD31 and Glut1 was not reduced (Figure S7D). Our results suggest that S1P released via *Mfsd2b* and *Spns2* is required for protection of CNS blood vessel integrity during embryonic development.

Compound deletion of *Mfsd2b* and *Spns2* impairs development of the aorta

S1P signaling is required for maturation and stabilization of blood vessels (Jung et al., 2012; Ben Shoham et al., 2012; Gaengel et al., 2012; Paik et al., 2004; Hubner et al., 2018). Therefore, we examined whether development of the descending aorta is affected in gDKO embryos. We found that the aortae of E13.5 gDKO embryos were deformed and often had flattened structures (Figure 5A). Nevertheless, they had a normal aortic circumferences compared with controls (Figures 5B and 5C). We observed that live gDKO embryos had a normal heartbeat. RBCs ($Ter119^+$ cells) were present in the aortic lumen, but to a lesser extent compared with controls, implying that blood flow was reduced in E13.5 gDKO embryos before death (Figure S8A). We found that the endothelial cell layer of the aorta, shown by staining with CD31, exhibited a disorganized pattern compared with controls (Figure 5A, arrowheads; Figures S9A and S9B). Next, the proliferation of endothelial cells was assessed by staining with Ki67 and ERG antibodies. Although we observed a trend of an increase in the number of $Ki67^+$ and ERG^+ cells in the vascular layers of the aorta of DKO embryos, this increase did not reach statistical significance (Figures S8B and S8C). Dead cells were not observed (Figure S9C). The coverage of smooth muscle cells is critical for maintenance of aortic structure. We found that expression of the smooth muscle cell marker α-SMA surrounding the aorta in the dorsal side was normal but that the layer itself was significantly thinner on the ventral side (Figures 5D and 5E). We found that the smooth muscle cell layer was less compacted with increased sizes of nuclei (Figure 5F, left panel, arrowheads). We observed that the arrangement of endothelial cells was also disorganized (Figure 5F, right panel, arrows), and disrupted expression of Claudin-5 in the aortic endothelium was observed (Figure 5F, red arrowheads). These results are consistent with the defects observed in the developing aorta of global S1P1 knockout embryos (Kono et al., 2004; Gaengel et al., 2012) but slightly less severe for the same developmental stage. This demonstrates that *Mfsd2b* and *Spns2* are required for S1P delivery to support the structural integrity of the developing aorta.

Mfsd2b and *Spns2* deficiency in Mx1Cre-sensitive cells sensitizes to anaphylactic shock and impairs peripheral but not CNS vasculature integrity

The significant reduction of plasma S1P of ctDKO-Mx1Cre mice described above prompted us to test whether mice with compound deficiency in *Mfsd2b* and *Spns2* are sensitized to anaphylactic shock. Upon histamine challenge, the core body temperature of control mice was decreased, but they re-gained body temperature within 25–30 min. In contrast, the core body temperature of ctDKO-Mx1Cre mice was decreased and remained low over 1 h (Figure 6A). Approximately 35% of ctDKO-Mx1Cre mice died, whereas none of the control mice died during histamine challenge (Figure 6B). The blood of ctDKO-Mx1Cre mice had slightly higher hematocrits and significantly higher amounts of histamine in plasma, reflecting plasma loss and impaired glomerular filtration (Figures 6C and 6D). Their systolic blood pressure under the histamine challenge was decreased significantly (Figure 6E). ctDKO-Mx1Cre mice were

(C) Number of RBCs in brain parenchyma of gDKO embryos in the GE regions. Each symbol represents one field from one embryo (n = 5 for controls and n = 6 for gDKO). Results are mean ± SD. **$p < 0.01$, t test.

(D and E) Diameter of blood vessels in GE (D) and midbrain (E) regions of E13.5 $Mfsd2b^{-/-}$ and gDKO. There is a significant increase in diameters of blood vessels in GE regions of gDKO embryos. Each symbol represents one vessel from 5–6 embryos per genotype.

Results are mean ± SD. *$p < 0.05$, Mann-Whitney U test. See also Figures S4 and S5.

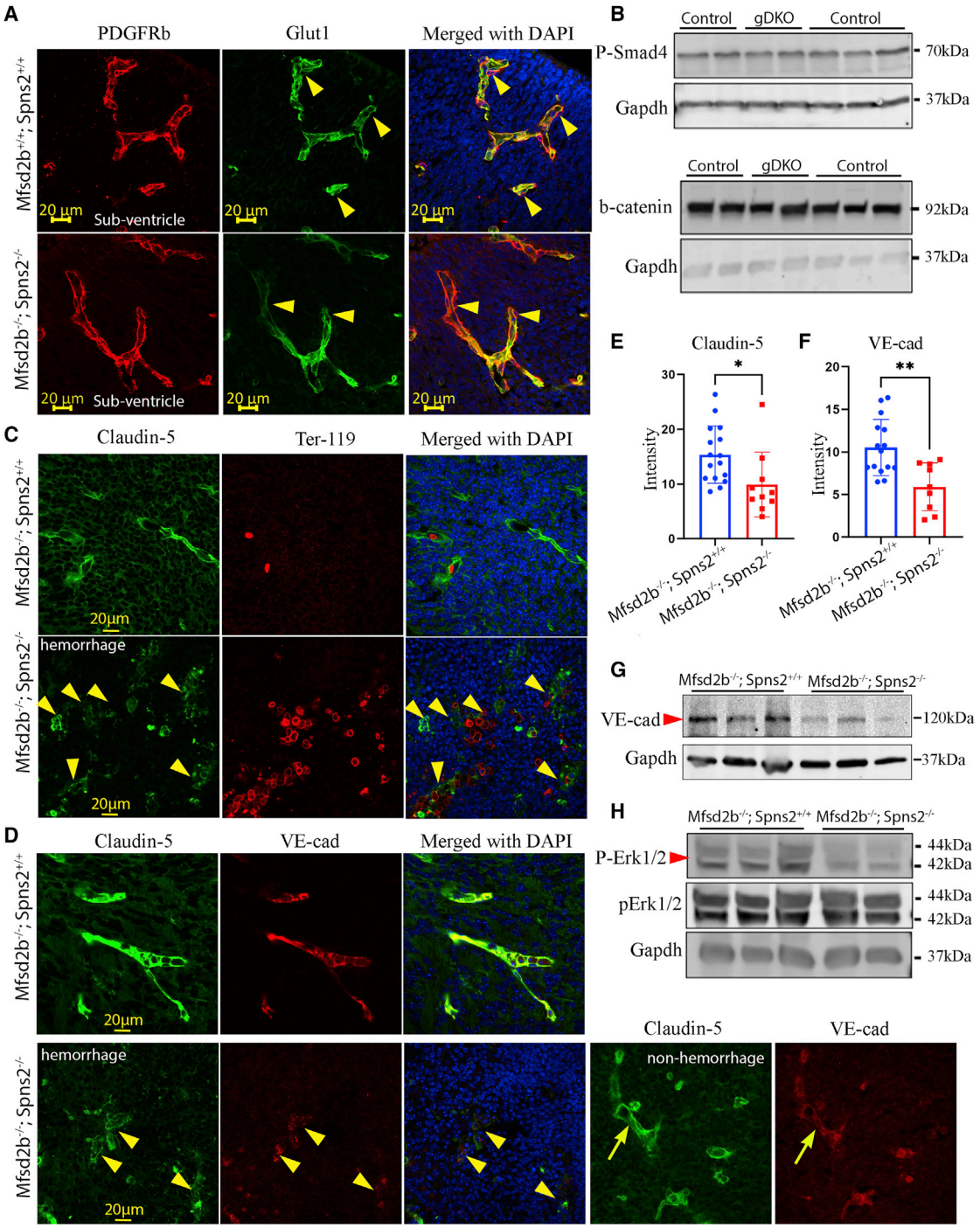

Figure 4. Lack of *Mfsd2b* and *Spns2* results in local rupture of CNS blood vessels during development

(A) Pericyte coverage was not reduced in CNS blood vessels of E13.5 gDKO embryos; n = 3 per genotype. Arrowheads indicate the pericyte cell body which is only stained with PDGFRb but not Glut1.

(B) Expression of canonical WNT (β-catenin) and TGF-β signaling (phosphorylated Smad4) proteins was comparable between E13.5 controls (*Mfsd2b*$^{-/-}$;*Spns2*$^{+/-}$ or *Mfsd2b*$^{-/-}$;*Spns2*$^{+/+}$) and E13.5 gDKO. n = 5 for controls, and n = 2 for gDKO.

(C) The expression pattern of Claudin-5 was disrupted in the ruptured cerebral blood vessels of E13.5 gDKO embryos. Arrowheads indicate the localization of Claudin-5; n = 3 per genotype.

(legend continued on next page)

more susceptible to platelet-activating factor (PAF) treatment (Figure 6F). To confirm that the significant reduction of plasma S1P in ctDKO-Mx1Cre mice explained the susceptibility to anaphylaxis, we performed rescue experiments where exogenous S1P was injected intravenously into ctDKO-Mx1Cre and control mice during histamine challenge. A bolus injection of S1P mitigated the core body temperature decrease in control and ctDKO-Mx1Cre mice, whereas vehicle treatment did not improve their low body temperature induced by histamine (Figure 6G). These data indicate that circulating S1P is required to maintain blood pressure during anaphylactic shock and that *Mfsd2b* and *Spns2* play a critical role in providing S1P to protect mice from the loss of vascular resistance induced by histamine challenge.

Next we examined whether the peripheral and CNS vasculature of ctDKO-Mx1Cre mice are permeable to Evans blue, a dye that binds to albumins when injected into the circulation. We showed that, under basal conditions, the lungs of ctDKO-Mx1Cre mice accumulated a slightly higher level of Evans blue, but the CNS vasculature of adult ctDKO-Mx1Cre mice was still intact (Figures S10A and S10B). To examine whether S1P from *Mfsd2b* and *Spns2* is required for blood-brain barrier integrity under histamine treatment, we intravenously injected Sulfo-NHS-Biotin, a small-molecule tracer, into ctDKO-Mx1Cre and control mice under histamine challenge. However, we did not observe significant extravasation of Sulfo-NHS-Biotin into the brain parenchyma of ctDKO-Mx1Cre mice (Figures S10C and S11A). These results indicate that S1P released from *Mfsd2b* and *Spns2* is dispensable for CNS vascular integrity under homeostasis and anaphylactic shock. In contrast, histological examination of the lungs of ctDKO-Mx1Cre mice after histamine challenge showed that pulmonary blood vessels of ctDKO-Mx1Cre mice were thickened, indicative of edema (Figure S10D, arrowheads). We also found that the airways of ctDKO-Mx1Cre mice were filled with RBCs, indicating that the lung vasculature of ctDKO-Mx1Cre mice was compromised under histamine treatment (Figure S10D, arrows). A similar loss of vascular integrity was observed in the lungs of ctDKO-Mx1Cre mice after PAF treatment (Figure S11B). To gain further insights into the reduced integrity of the pulmonary vasculature in ctDKO-Mx1Cre mice, we examined the expression levels of tight junction proteins. We found that expression of Occludin and Claudin-5 was reduced in the lungs of ctDKO-Mx1Cre mice, whereas expression of PLVAP was unaltered (Figures S10E and S10F). Expression of N-cadherin 5 was increased, perhaps to compensate for the decreased expression of tight junction proteins (Figures S10E and S10F). We also examined whether treatment with the S1P1-selective agonist SEW2871 could reduce Evans blue leakage in the lungs of ctDKO-Mx1Cre mice. However, SEW2871 slightly exacerbated pulmonary leakage, suggesting its functional antagonism (Figures S12A–S12C). Our results reveal that S1P released from *Mfsd2b* and *Spns2* in Mx1Cre-sensitive cells is required for the integrity of the lungs but not the CNS vasculature in adult mice. Our results indicate that the proportion of plasma S1P provided by *Mfsd2b* and *Spns2* is essential for maintenance of vascular integrity and vascular tone.

Mfsd2b and *Spns2* may not account for all S1P release to plasma from Mx1Cre-sensitive cells

We noted that the pulmonary leakage in ctDKO-Mx1Cre mice appeared to be milder compared with that reported for SphK1$^{f/-}$;SphK2$^{f/-}$Mx1Cre mice (Gazit et al., 2016; Camerer et al., 2009). This could be linked to the incomplete reduction of plasma S1P in ctDKO-Mx1Cre mice (Figure 2I). To gain further insights, we compared plasma S1P levels from ctDKO-Mx1Cre and SphK1$^{f/-}$;SphK2$^{f/-}$Mx1Cre (hereafter ckDKO-Mx1Cre) mice (Figures 7A and 7B). Our lipidomic results indeed showed that mice lacking *Mfsd2b* and *Spns2* still had higher levels of plasma S1P (~65% reduction) compared with ckDKO-Mx1Cr mice (~98% reduction). These results suggest an additional source of plasma S1P that is independent of *Mfsd2b* and *Spns2* among Mx1Cre-sensitive cells (Figure 7C). To ascertain that plasma S1P can still be synthesized and released in ctDKO-Mx1Cre mice, we injected radioactive [3-^{3}H] sphingosine (d18:1 sphingosine) into the circulation of ctDKO-Mx1Cre and control mice (Figures 7D and 7E). Then the amount of [3-^{3}H] S1P released into plasma and accumulated in RBCs was analyzed within 2 h after injection. In control mice, [3-^{3}H] S1P was detected in plasma within 10 min after [3-^{3}H] sphingosine injection (Figures 7D and 7E) and decreased gradually over time (Figure 7D). In ctDKO-Mx1Cre mice, although significantly less plasma [3-^{3}H] S1P was found 10 min after [3-^{3}H] sphingosine injection, a detectable level of S1P was still observed in the plasma of ctDKO-Mx1Cre mice (Figure 7D). This source of S1P is independent of RBC as [3-^{3}H] S1P was accumulated in RBC from ctDKO-Mx1Cre mice, whereas it was secreted from wild-type (WT) RBC over time (Figure 7E). Plasma S1P production is increased in response to irradiation or chemotherapy. We tested whether irradiation would increase plasma S1P in ctDKO-Mx1Cre mice. We found that sub-lethal dose of irradiation (6.5 Gy) significantly increased plasma S1P production in control mice (SphK1$^{f/-}$; SphK2$^{f/-}$ or Mfsd2b$^{f/f}$;Spns2$^{f/f}$, without Mx1Cre) (Figures 7F and 7G). Although irradiation-increased plasma S1P was largely dependent on *Mfsd2b* and *Spns2*, quantitatively, a small amount of plasma S1P was increased in ctDKO-Mx1Cre mice (0.29 versus 0.41 μM) but not in ckDKO-Mx1Cre mice (0.022 versus 0.046 μM) (Figures 7F and 7G). The low level of plasma S1P in ckDKO-Mx1Cre was unlikely to be due to increased S1P degradation by S1P lyase (Figures S13A–S13C). These results indicate

(D) The expression pattern of VE-cadherin was dysregulated in ruptured cerebral blood vessels of E13.5 gDKO embryos. Arrowheads indicate the localization of VE-Cadherin; n = 3 per genotype.
(E and F) Reduced immunostaining signals of Claudin-5 and VE-cadherin in the hemorrhagic regions of E13.5 gDKO compared with controls. n = 3 per genotype.
(G), Reduced expression of VE-cadherin in the whole brain lysates from E13.5 gDKO compared with controls. n = 3 per genotype.
(H) Reduced expression of phosphorylated ERK1/2 protein from whole-brain lysates of E13.5 gDKO compared with controls. n = 3 for control, and n = 2 for gDKO embryos. n = 3 per genotype.
Results are mean ± SD, *p < 0.05, **p < 0.01, t test. See also Figures S6 and S7.

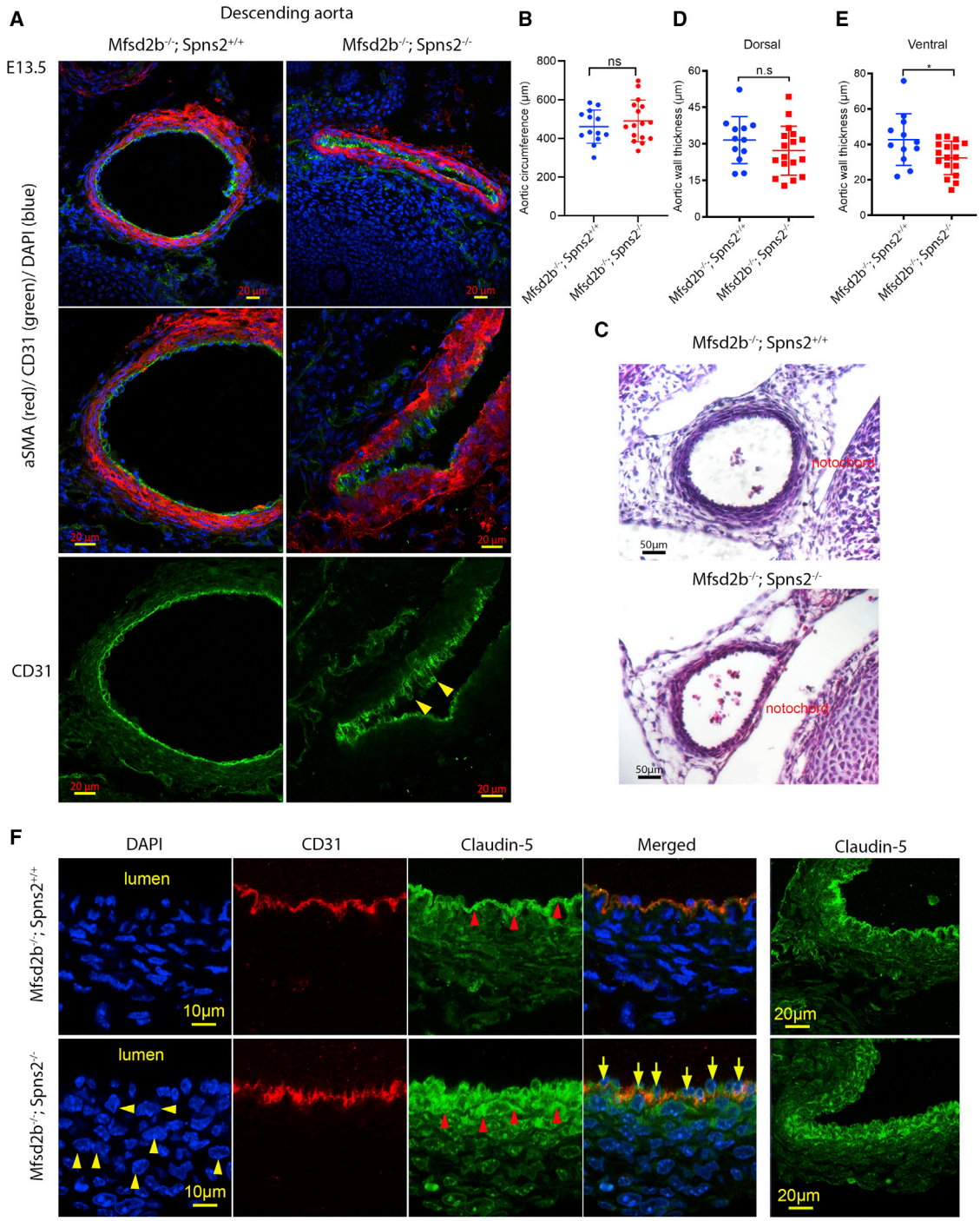

Figure 5. Defects in aortic structures in gDKO embryos

(A) Aortae of gDKO embryos were deformed. Shown are representative images of the localization of smooth muscle cells (α-SMA, red) and endothelial cells (CD31, green) in the descending aorta of E13.5 control (*Mfsd2b*$^{-/-}$) and gDKO embryos.

(B) Measurement of the circumference of aortae from control (*Mfsd2b*$^{-/-}$) and gDKO embryos. Each symbol represents one aorta from 9–10 embryos per genotype. Results are mean and SD; ns, not significant. t test.

(C) Representative H&E images of aortae from control and gDKO embryos.

(legend continued on next page)

that ctDKO-Mx1Cre mice retain the capacity to release a minor amount of S1P.

Monocytes have been reported to provide S1P in lymph nodes in response to inflammation (Baeyens et al., 2021). We explored the possibility that the additional source of S1P is released from myeloid cells. Thus, we depleted myeloid cells, including neutrophils and monocytes, using an Ly6C/G antibody (Figure 7H). Mice treated with the Ly6C/G antibody had significantly lower WBC counts, indicating that the treatment was effective (Figure 7H). However, the levels of plasma S1P from ctDKO-Mx1Cre and control mice before and after Ly6C/G treatment were not reduced (Figure 7I). Although ctDKO-Mx1Cre mice had slightly basal leakage of Evans blue in the lungs (Figures S10A and S10B), Evans blue leakage in the lungs of myeloid-depleted ctDKO-Mx1Cre mice was not elevated (Figures 7J and 7K). Our results show that, although *Mfsd2b*- and *Spns2*-expressing cells provide most of the plasma S1P, a minor amount of the lipid mediator is provided by Mx1Ce-sensitive cells independent of these transporters.

DISCUSSION

S1P plays an essential signaling role in the cardiovascular system, particularly for maintaining blood vessel health. It is the extracellular ligand for 5 cognate G-protein-coupled receptors (S1P1–S1P5). The essential roles of S1P in the vasculature have been established via pharmacological or genetic perturbation of S1P receptors or SphK1 and SphK2. Among the receptors, S1P1 is highly expressed in endothelial cells and plays a particularly important role in regulation of endothelial cell functions by sensing the circulating S1P. Mice lacking S1P1 or SphK1 and SphK2 are embryonically lethal because of severe hemorrhage (Liu et al., 2000; Mizugishi et al., 2005). Postnatal ablation of S1P1 in endothelial cells or compound conditional deletion of SphK1/2 also causes blood vessel leakage, especially in the pulmonary vasculature (Gazit et al., 2016; Yanagida et al., 2017; Camerer et al., 2009). The common view of S1P signaling is that S1P is synthesized in cells and then exported to the extracellular milieu for signaling functions. Several cell types, including endothelial cells and blood cells, including erythrocytes, can release S1P via the two recently identified S1P exporters *Mfsd2b* and *Spns2*. Extracellular SphK1 has been reported to generate S1P in the circulation (Venkataraman et al., 2006). Adding to the complexity of S1P sources, several ABC transporters have been reported to harbor the capacity for S1P transport (Mitra et al., 2006; Kobayashi et al., 2009; Vogt et al., 2018). Our results show that mice lacking *Mfsd2b* and *Spns2* die during gestation. Thus, S1P exported by *Mfsd2b* and *Spns2* is critical for embryonic development. We show in adult mice that *Mfsd2b* and *Spns2* are responsible for release of approximately 80% of plasma S1P, which is produced by SphK1 and SphK2 in Mx1Cre-sensitive cells, including hematopoietic and endothelial cells. This indicates that there may be an Mx1Cre-sensitive cell type that contributes a minor fraction of plasma S1P independent of *Mfsd2b* and *Spns2*.

S1P is synthesized in most cells in the body. However, only a few cell types are known to export S1P. Identifying the sources of S1P is critical for understanding how it regulates immune and blood vessel functions. We determined that *Mfsd2b*, which is expressed in blood cells, contributes approximately half of the plasma S1P (Vu et al., 2017). Among *Mfsd2b*-positive cells, erythrocytes and platelets have been shown to provide plasma S1P (Chandrakanthan et al., 2021; Nguyen et al., 2020; Tan et al., 2020). S1P is also released via *Spns2*, but the amount of plasma S1P contributed by *Spns2* varies in different studies (Fukuhara et al., 2012; Mendoza et al., 2012; Nagahashi et al., 2013). In our analyses, we found that global deletion of *Spns2* results in a 10%–20% reduction of plasma S1P. This is similar to what has been reported after deletion of the transporter in endothelial cells (Mendoza et al., 2012). Lack of *Spns2* causes severe lymphopenia, suggesting that this transporter provides most of the S1P in lymph. These findings suggest that *Spns2* provides S1P from cellular sources distinct from *Mfsd2b*, in particularly from lymphatic endothelial cells. Our data show that embryos lacking *Mfsd2b* and *Spns2* die between E13.4 and E14.5. The lethality of embryos lacking *Mfsd2b* and *Spns2* is slightly delayed compared with DKO of SphKs but largely recapitulates the phenotype of the S1P1 knockout. These results suggest that *Mfsd2b* and *Spns2* coordinate to deliver S1P to S1P1 during embryonic development. Our results also argue against the roles of other S1P exporters, notably ATP transporters, during embryonic development (Mitra et al., 2006; Takabe et al., 2010; Sato et al., 2007).

Global knockout of S1P1 or SphK1 and SphK2 embryos exhibit severe hemorrhage and defects in the developing aorta (Liu et al., 2000; Mizugishi et al., 2005). Embryos lacking *Mfsd2b* and *Spns2* also have hemorrhage throughout the body, especially in the lower dorsal regions. A main role of S1P signaling in endothelial cells is to inhibit VEGF-induced tip cell formation and angiogenic hypersprouting and stabilize adherens junctions. We observed that the compound transporter knockouts exhibit defective aortic structures in which the organization of the endothelial cell layer and the expression pattern of Claudin-5 were dysregulated. We did not observe a significant reduction of the number of smooth muscle cells in the aorta. Instead, their coverage in the aortae was less compacted. Blood cells were also observed in the aortic lumen but with lower levels compared with controls, which suggests that blood flow was reduced before death. These phenotypes might explain the deformed aortic structures

(D and E) Thickness of the α-SMA layer from dorsal (D) and ventral (E) sides. Each symbol represents one aorta from 9–10 embryos per genotype. Results are mean and SD. *$p < 0.05$, t test.

(F) Defects in the endothelial layer of aortae of E13.5 gDKO embryos (arrows). Claudin-5 was also expressed ectopically in the vascular smooth muscle cell layer (red arrowheads). Nuclei of smooth muscle cells in aortae of E13.5 gDKO embryos exhibited round structures (left panel, arrowheads) compared with condensed structures of controls. Right panels: low-magnification images of Claudin-5 staining of aortae from control and gDKO. Experiments were performed from 4–5 embryos per genotype.

See also Figures S8 and S9.

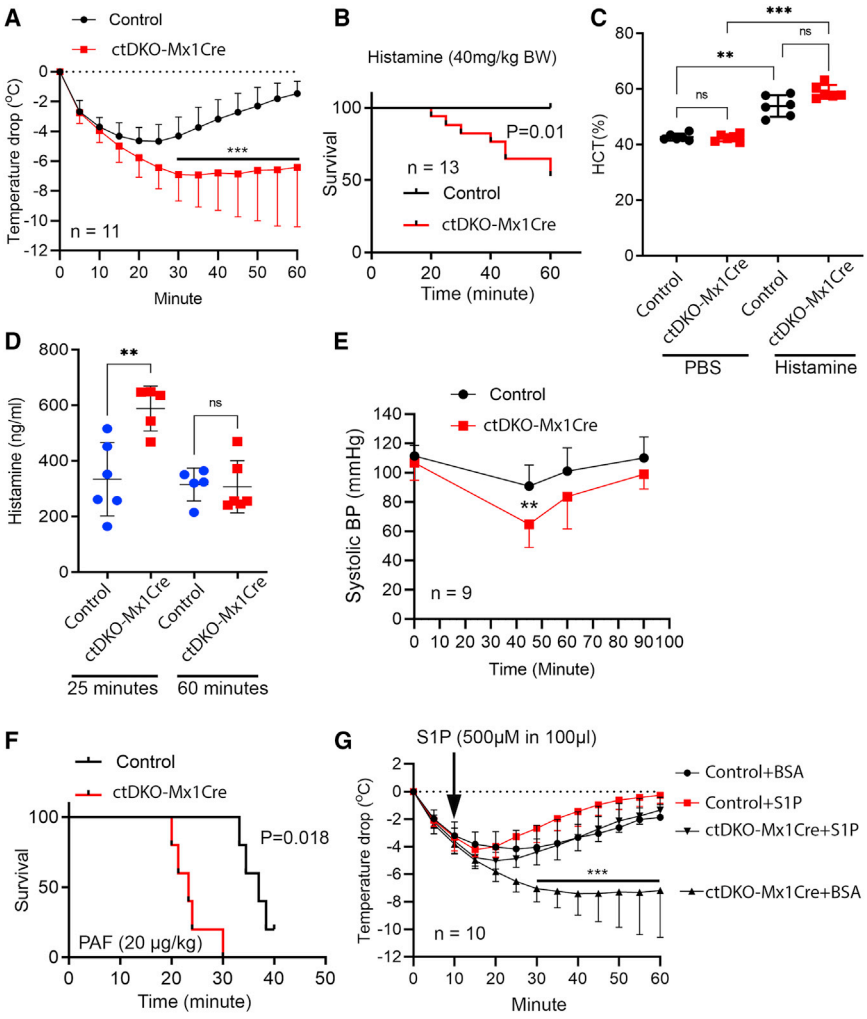

Figure 6. The sources of circulating S1P from *Mfsd2b* and *Spns2* are required for protection from anaphylactic shock

(A) Core body temperature drop in control and ctDKO-Mx1Cre mice (n = 11, 3–4 months old) after histamine challenge.

(B) Survival curve of male control and ctDKO-Mx1Cre mice during histamine challenge. Seven of 20 ctDKO-Mx1Cre mice died, whereas all control mice survived (n = 13 for WT, n = 20 for ctDKO-Mx1Cre mice from 4 experiments).

(C) Hematocrit (HCT) of control and ctDKO-Mx1Cre mice, measured after 25 min of histamine challenge (n = 6 per genotype from 2 experiments).

(D) Histamine levels in plasma of control and ctDKO-Mx1Cre mice 25 and 60 min after intravenous injection of histamine. Each symbol represents one mouse (n = 4–5 per genotype).

(E) Systolic blood pressure was monitored in control and ctDKO-Mx1Cre mice before (0 min) and 45, 60, and 90 min after histamine challenge.

(F) Survival curve of control and ctDKO-Mx1Cre mice after PAF injection; n = 5 per genotype.

(G) Exogenous administration of S1P rescued core temperature drop during anaphylaxis in ctDKO-Mx1Cre mice (n = 10 per genotype, four experiments).

Results are mean ± SD. $^{**}p < 0.01$, $^{***}p < 0.001$. One or two-way ANOVA was used. See also Figures S10–S12.

observed in the DKO embryos. These findings point to a role of *Mfsd2b* and *Spns2* in delivering S1P from SphK1 and SphK2 to S1P receptors, especially S1P1, for maintenance of the peripheral vasculature. In the developing brain, lack of *Mfsd2b* and *Spns2* causes ruptured blood vessels in which extravasation of RBCs was seen in several brain regions. S1P receptors sense S1P at nanomolar concentrations and are expressed mainly on the luminal side of developing blood vessels. Accordingly, isolated deletion of *Spns2*, which is mainly expressed in endothelial cells, is insufficient to cause these vascular phenotypes in the brain. *Mfsd2b* is expressed in primitive RBCs. Thus, it can only contribute to the circulating S1P. These findings imply that, during development, *Mfsd2b* and *Spns2* release S1P into the circulation, which is sensed by S1P receptors in nascent blood vessels for maturation and stabilization of developing vasculature. It has been shown that *Mfsd2a* forms a complex with *Spns2* to maintain the function of the blood-brain barrier (Wang et al., 2020). *Mfsd2a* is expressed in the blood-brain barrier early during development (Nguyen et al., 2014; Ben-Zvi et al., 2014). However, the presence of *Mfsd2a* is insufficient to rescue the lethality of *Mfsd2b* and Spns2 knockout embryos, arguing against its role as an S1P transporter.

Plasma S1P concentration in adult humans and mice is in a range of 1–2 μM, which exceeds the levels of S1P required for receptor activation (K_d = 10–50 nM) (Lee et al., 1998). Conditional deletion of S1P1 in endothelial cells results in vascular leakage in the lungs as well as the brain. Mice deficient for plasma S1P by compound deletion of SphK1 and SphK2 only exhibit pulmonary leakage with Evans blue (Gazit et al., 2016; Camerer et al., 2009). In line with the results from SphK1 and SphK2 knockouts, the pulmonary vasculature of mice lacking *Mfsd2b* and *Spns2* was also leaky to Evans blue but with lesser severity. In mice with compound loss of SphK1 and SphK2, the plasma concentration of S1P is approximately 20 nM, whereas plasma S1P in the compound knockout of *Mfsd2b* and *Spns2* mice is still more than 200 nM. A reduction of 50% plasma S1P in ApoM knockout mice is sufficient to cause pulmonary leakage of Evans blue (Christensen et al., 2016). Thus, it seems that the concentration of S1P needed for activation of S1P receptors to protect peripheral vasculature is higher than that shown *in vitro* (Lee et al., 1998). It also appears that high levels of circulating S1P are needed for activation of S1P receptors in perivascular cells for maintenance of vascular tone (Olivera et al., 2010; Gazit et al., 2016). In contrast to the lung vasculature, cerebral blood vessels of adult ctDKO-Mx1Cre or ckDKO-Mx1Cre mice are intact, suggesting that the remaining amount of S1P is sufficient to sustain the blood-brain barrier integrity or that there is a different source of S1P important for S1P1

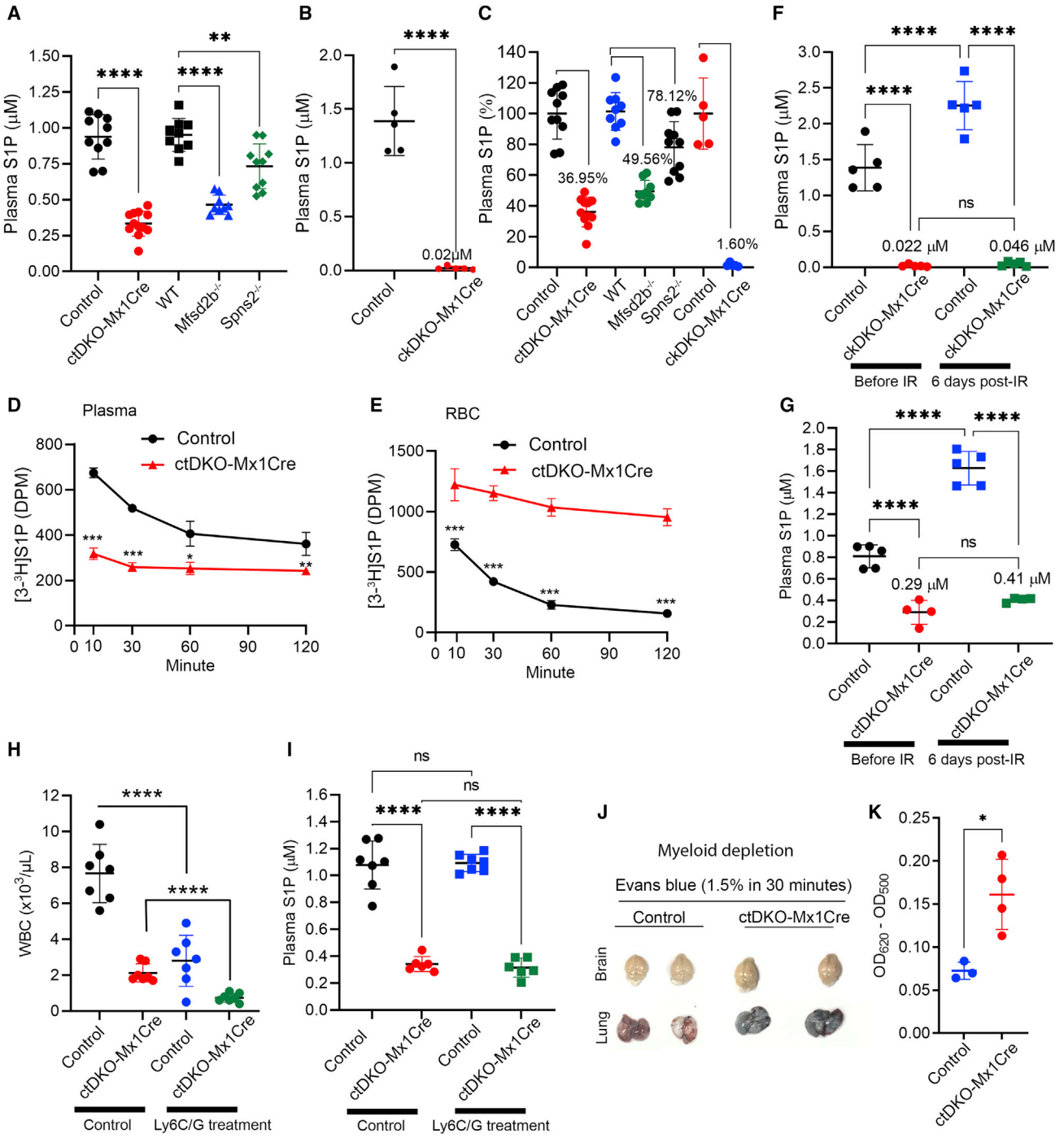

Figure 7. *Mfsd2b* and *Spns2* provide the majority of plasma S1P, but a minor fraction of plasma S1P is independent of these transporters

(A and B) Comparison of plasma S1P levels from ctDKO-Mx1Cre and ckDKO-Mx1Cre (SphK1$^{f/-}$, SphK2$^{f/-}$ Mx1Cre) mice with their respective controls. Each symbol represents one mouse; n = 4–5 per genotype.

(C) Percentage of plasma S1P from indicated genotypes. Each symbol represents one mouse; n = 4–5 per genotype. Results are mean ± SD, ****p < 0.0001, ***p < 0.001, *p < 0.05. One-way ANOVA was used in (A). A t test was used for (B).

(D and E) *In vivo* S1P transport assay from control and ctDKO-Mx1Cre mice. Shown are [3-^{3}H] S1P levels in plasma (D) and erythrocytes (E) of ctDKO-Mx1Cre and control mice 10, 30, 60, and 120 min after injection of [3-^{3}H] sphingosine; n = 4 per genotype from two experiments. Results are mean ± SD; ***p < 0.001, **p < 0.01, *p < 0.05. Two-way ANOVA was used.

(legend continued on next page)

activation in the neurovascular unit. This remains to be determined. Circulating S1P is required for protection of mice undergoing anaphylactic shock. We found that, although ctDKO-Mx1Cre mice retained approximately 20% of normal plasma S1P, they exhibited severe susceptibility to anaphylactic shock, indicating that high plasma S1P provided by *Mfsd2b* and *Spns2* is essential for maintaining vascular functions during pathological conditions. Supplementation of exogenous S1P to the circulation was sufficient to abolish the susceptibility to anaphylaxis in the knockout mice. Therefore, these findings emphasize the importance of having high plasma S1P concentrations that exceed the levels needed for S1P receptor activation.

We found that compound knockout of *Mfsd2b* and *Spns2* using Mx1Cre causes a maximal reduction of 80% plasma S1P, whereas a similar deletion of SphK1 and SphK2 reduces plasma S1P by 98%. These results may suggest that there is a minor source of plasma S1P that is independent of *Mfsd2b* and *Spns2* among Mx1Cre-sensitive cells. Deletion of SphK1 and SphK2 or *Spns2* in endothelial cells only reduces 0%–20% of plasma S1P (Gazit et al., 2016; Mendoza et al., 2012). This argues against a role of endothelial cells for the source of S1P. A recent study suggests that inflammatory monocytes secrete S1P during immune responses (Baeyens et al., 2021). Nevertheless, depletion of neutrophils and monocytes using the Ly6C/G antibody failed to abolish the remaining amount of plasma S1P in *Mfsd2b* and *Spns2* DKO mice, implying that other blood cells, such as mast cells or eosinophils, could be involved. Identification of such a cell type and the transporter responsible for this source of S1P should provide a better understanding of how different sources of S1P regulate its receptor signaling. Alternatively, although our results show that a minor fraction of plasma S1P is produced from circulating sphingosines in ctDKO-Mx1Cre mice, massive overload of S1P in erythrocytes because of *Mfsd2b* inhibition could force S1P leakage in non-physiological mechanisms. Future investigations of the additional source of circulating S1P would be required.

Our study shows that *Mfsd2b* and *Spns2* are the two major S1P transporters that secure S1P signaling during vasculature development. These transporters, expressed in hematopoietic and endothelial cells, also provide a major fraction of plasma S1P required for maintenance of vascular functions under homeostasis and in response to systemic vascular challenge.

Limitations of the study

Although our results show that reduced expression of tight junction proteins is responsible for the hemorrhage observed in DKO of *Mfsd2b* and *Spns2*, we are not able to show that the tight junctions between endothelial cells are ruptured. Our results only suggest that there is an additional source of plasma S1P independent of *Mfsd2b* and *Spns2*. This notion will need further investigation and validation.

STAR★METHODS

Detailed methods are provided in the online version of this paper and include the following:

- KEY RESOURCES TABLE
- RESOURCE AVAILABILITY
  - Lead contact
  - Materials availability
  - Data and code availability
- EXPERIMENTAL MODEL AND SUBJECT DETAILS
  - Mice
- METHOD DETAILS
  - Chemicals
  - Antibodies
  - Complete blood count
  - Quantitative PCR
  - Immunohistochemistry
  - Transport assay with red blood cells
  - *In vivo* transport assay with [3-^{3}H] sphingosine
  - Western blot analysis
  - Plasma collection for lipidomic analysis
  - Lipidomics
  - Body temperature measurements
  - Blood pressure measurements
  - Histamine clearance
  - Sulfo-NHS-biotin extravasation
  - Paraffin sections
  - Myeloid cell depletion
  - Evans blue extravasation
  - Drug treatment
  - Irradiation
- QUANTIFICATION AND STATISTICAL ANALYSIS
  - Quantification of immunostaining
  - Blood vessel density
  - Statistical analysis

SUPPLEMENTAL INFORMATION

Supplemental information can be found online at https://doi.org/10.1016/j.celrep.2022.111208.

ACKNOWLEDGMENTS

This study was supported in part by Singapore Ministry of Health's National Research Council NMRC/OFIRG/0066/20, Ministry of Education

(F and G) Plasma S1P levels from controls, ckDKO-Mx1Cre, and ctDKO-Mx1Cre mice before (day 0) and 6 days after irradiation with 6.5 Gy. The samples before irradiation in (F) and (G) were the same as in (A) and (B). Each symbol represents one mouse; n = 4–5 per genotype. Results are mean ± SD; ****$p < 0.0001$, ***$p < 0.001$. one-way ANOVA was used.

(H and I) Depletion of myeloid cells from control and ctDKO-Mx1Cre mice. The WBC count was reduced in control and ctDKO-Mx1Cre mice after 40-h treatment with the Ly6C/G antibody. Plasma S1P levels in control or ctDKOMx1Cre mice treated with the Ly6C/G antibody were comparable with the same genotype without treatment. Each symbol represents one mouse; n = 6–7 per genotype. Results are mean ± SD; ****$p < 0.0001$, *$p < 0.05$. A t test (H) and one-way ANOVA (I) were used.

(J and K) Accumulation of Evans blue in the lungs of control and ctDKO-Mx1Cre mice 40 h after treatment with the Ly6C/G antibody. Results are mean ± SD, *$p < 0.05$.

See also Figure S13.

MOE2018-T2-1-126, and NUSMED-FOS Joint Research Programme on Healthy Brain Aging grants (to L.N.N.) and the French National Research Agency (ANR-19-CE14-0028 to E.C.).

AUTHOR CONTRIBUTIONS

T.N.U.L., T.Q.N., P.K., C.K.H.T., and F.T. performed *in vivo* experiments and *ex vivo* experiments. Z.H. and Y.T.K.N. performed H&E staining. L.C. and I.D.G. performed experiments with SphK1/2 knockouts. E.C. designed experiments in SphK1/2 knockouts and edited the manuscript. M.R.W. and A.C.-G. supervised lipidomics methodology. T.Q.N. performed lipidomics analysis. V.K.S. helped with Evans blue experiments. L.N.N. and T.N.U.L. performed confocal imaging. L.N.N. conceived and designed the study and experiments and wrote the paper. We thank Dr. Sangha Baik for initial work on the project.

DECLARATION OF INTERESTS

The authors declare no competing interests.

Received: August 20, 2021
Revised: May 23, 2022
Accepted: July 21, 2022
Published: August 16, 2022

REFERENCES

Arnold, T.D., Niaudet, C., Pang, M.F., Siegenthaler, J., Gaengel, K., Jung, B., Ferrero, G.M., Mukouyama, Y.S., Fuxe, J., Akhurst, R., et al. (2014). Excessive vascular sprouting underlies cerebral hemorrhage in mice lacking alphaV-beta8-TGFbeta signaling in the brain. Development *141*, 4489–4499.

Baeyens, A., Bracero, S., Chaluvadi, V.S., Khodadadi-Jamayran, A., Cammer, M., and Schwab, S.R. (2021). Monocyte-derived S1P in the lymph node regulates immune responses. Nature *592*, 290–295.

Ben Shoham, A., Malkinson, G., Krief, S., Shwartz, Y., Ely, Y., Ferrara, N., Yaniv, K., and Zelzer, E. (2012). S1P1 inhibits sprouting angiogenesis during vascular development. Development *139*, 3859–3869.

Ben-Zvi, A., Lacoste, B., Kur, E., Andreone, B.J., Mayshar, Y., Yan, H., and Gu, C. (2014). Mfsd2a is critical for the formation and function of the blood-brain barrier. Nature *509*, 507–511.

Camerer, E., Regard, J.B., Cornelissen, I., Srinivasan, Y., Duong, D.N., Palmer, D., Pham, T.H., Wong, J.S., Pappu, R., and Coughlin, S.R. (2009). Sphingosine-1-phosphate in the plasma compartment regulates basal and inflammation-induced vascular leak in mice. J. Clin. Invest. *119*, 1871–1879.

Cao, J., Spielmann, M., Qiu, X., Huang, X., Ibrahim, D.M., Hill, A.J., Zhang, F., Mundlos, S., Christiansen, L., Steemers, F.J., et al. (2019). The single-cell transcriptional landscape of mammalian organogenesis. Nature *566*, 496–502.

Chandrakanthan, M., Nguyen, T.Q., Hasan, Z., Muralidharan, S., Vu, T.M., Li, A.W.L., Le, U.T.N., Thi Thuy Ha, H., Baik, S.H., Tan, S.H., et al. (2021). Deletion of Mfsd2b impairs thrombotic functions of platelets. Nat. Commun. *12*, 2286.

Cho, C., Smallwood, P.M., and Nathans, J. (2017). Reck and Gpr124 are essential receptor cofactors for Wnt7a/Wnt7b-specific signaling in mammalian CNS angiogenesis and blood-brain barrier regulation. Neuron *95*, 1056–1073.e5.

Christensen, P.M., Liu, C.H., Swendeman, S.L., Obinata, H., Qvortrup, K., Nielsen, L.B., Hla, T., Di Lorenzo, A., and Christoffersen, C. (2016). Impaired endothelial barrier function in apolipoprotein M-deficient mice is dependent on sphingosine-1-phosphate receptor 1. Faseb. J. *30*, 2351–2359.

Crist, A.M., Zhou, X., Garai, J., Lee, A.R., Thoele, J., Ullmer, C., Klein, C., Zabaleta, J., and Meadows, S.M. (2019). Angiopoietin-2 inhibition rescues arteriovenous malformation in a Smad4 hereditary hemorrhagic telangiectasia mouse model. Circulation *139*, 2049–2063.

Daneman, R., Agalliu, D., Zhou, L., Kuhnert, F., Kuo, C.J., and Barres, B.A. (2009). Wnt/beta-catenin signaling is required for CNS, but not non-CNS, angiogenesis. Proc. Natl. Acad. Sci. USA *106*, 641–646.

Dave, J.M., Mirabella, T., Weatherbee, S.D., and Greif, D.M. (2018). Pericyte ALK5/TIMP3 Axis contributes to endothelial morphogenesis in the developing brain. Dev. Cell *47*, 388–389.

Fukuhara, S., Simmons, S., Kawamura, S., Inoue, A., Orba, Y., Tokudome, T., Sunden, Y., Arai, Y., Moriwaki, K., Ishida, J., et al. (2012). The sphingosine-1-phosphate transporter Spns2 expressed on endothelial cells regulates lymphocyte trafficking in mice. J. Clin. Invest. *122*, 1416–1426.

Gaengel, K., and Betsholtz, C. (2013). Endocytosis regulates VEGF signalling during angiogenesis. Nat. Cell Biol. *15*, 233–235.

Gaengel, K., Niaudet, C., Hagikura, K., Laviña, B., Siemsen, B.L., Muhl, L., Hofmann, J.J., Ebarasi, L., Nyström, S., Rymo, S., et al. (2012). The sphingosine-1-phosphate receptor S1PR1 restricts sprouting angiogenesis by regulating the interplay between VE-cadherin and VEGFR2. Dev. Cell *23*, 587–599.

Gao, L., Ji, S., Burla, B., Wenk, M.R., Torta, F., and Cazenave-Gassiot, A. (2021). LICAR: an application for isotopic correction of targeted lipidomic data acquired with class-based chromatographic separations using multiple reaction monitoring. Anal. Chem. *93*, 3163–3171.

Gazit, S.L., Mariko, B., Thérond, P., Decouture, B., Xiong, Y., Couty, L., Bonnin, P., Baudrie, V., Le Gall, S.M., Dizier, B., et al. (2016). Platelet and erythrocyte sources of S1P are redundant for vascular development and homeostasis, but both rendered essential after plasma S1P depletion in anaphylactic shock. Circ. Res. *119*, e110–e126.

Hla, T., and Dannenberg, A.J. (2012). Sphingolipid signaling in metabolic disorders. Cell Metab. *16*, 420–434.

Hubner, K., Cabochette, P., Dieguez-Hurtado, R., Wiesner, C., Wakayama, Y., Grassme, K.S., Hubert, M., Guenther, S., Belting, H.G., Affolter, M., et al. (2018). Wnt/beta-catenin signaling regulates VE-cadherin-mediated anastomosis of brain capillaries by counteracting S1pr1 signaling. Nat. Commun. *9*, 4860.

Jo, E., Sanna, M.G., Gonzalez-Cabrera, P.J., Thangada, S., Tigyi, G., Osborne, D.A., Hla, T., Parrill, A.L., and Rosen, H. (2005). S1P1-selective in vivo-active agonists from high-throughput screening: off-the-shelf chemical probes of receptor interactions, signaling, and fate. Chem. Biol. *12*, 703–715.

Jung, B., Obinata, H., Galvani, S., Mendelson, K., Ding, B.S., Skoura, A., Kinzel, B., Brinkmann, V., Rafii, S., Evans, T., and Hla, T. (2012). Flow-regulated endothelial S1P receptor-1 signaling sustains vascular development. Dev. Cell *23*, 600–610.

Kobayashi, N., Kobayashi, N., Yamaguchi, A., and Nishi, T. (2009). Characterization of the ATP-dependent sphingosine 1-phosphate transporter in rat erythrocytes. J. Biol. Chem. *284*, 21192–21200.

Kono, M., Mi, Y., Liu, Y., Sasaki, T., Allende, M.L., Wu, Y.P., Yamashita, T., and Proia, R.L. (2004). The sphingosine-1-phosphate receptors S1P1, S1P2, and S1P3 function coordinately during embryonic angiogenesis. J. Biol. Chem. *279*, 29367–29373.

Kühn, R., Schwenk, F., Aguet, M., and Rajewsky, K. (1995). Inducible gene targeting in mice. Science *269*, 1427–1429.

Lee, M.J., Van Brocklyn, J.R., Thangada, S., Liu, C.H., Hand, A.R., Menzeleev, R., Spiegel, S., and Hla, T. (1998). Sphingosine-1-phosphate as a ligand for the G protein-coupled receptor EDG-1. Science *279*, 1552–1555.

Li, F., Lan, Y., Wang, Y., Wang, J., Yang, G., Meng, F., Han, H., Meng, A., Wang, Y., and Yang, X. (2011). Endothelial Smad4 maintains cerebrovascular integrity by activating N-cadherin through cooperation with Notch. Dev. Cell *20*, 291–302.

Lindahl, P., Johansson, B.R., Levéen, P., and Betsholtz, C. (1997). Pericyte loss and microaneurysm formation in PDGF-B-deficient mice. Science *277*, 242–245.

Liu, Y., Wada, R., Yamashita, T., Mi, Y., Deng, C.X., Hobson, J.P., Rosenfeldt, H.M., Nava, V.E., Chae, S.S., Lee, M.J., et al. (2000). Edg-1, the G protein-coupled receptor for sphingosine-1-phosphate, is essential for vascular maturation. J. Clin. Invest. *106*, 951–961.

Mendoza, A., Bréart, B., Ramos-Perez, W.D., Pitt, L.A., Gobert, M., Sunkara, M., Lafaille, J.J., Morris, A.J., and Schwab, S.R. (2012). The transporter

Spns2 is required for secretion of lymph but not plasma sphingosine-1-phosphate. Cell Rep. *2*, 1104–1110.

Mitra, P., Oskeritzian, C.A., Payne, S.G., Beaven, M.A., Milstien, S., and Spiegel, S. (2006). Role of ABCC1 in export of sphingosine-1-phosphate from mast cells. Proc. Natl. Acad. Sci. USA *103*, 16394–16399.

Mizugishi, K., Yamashita, T., Olivera, A., Miller, G.F., Spiegel, S., and Proia, R.L. (2005). Essential role for sphingosine kinases in neural and vascular development. Mol. Cell Biol. *25*, 11113–11121.

Nagahashi, M., Kim, E.Y., Yamada, A., Ramachandran, S., Allegood, J.C., Hait, N.C., Maceyka, M., Milstien, S., Takabe, K., and Spiegel, S. (2013). Spns2, a transporter of phosphorylated sphingoid bases, regulates their blood and lymph levels, and the lymphatic network. FASEB J. *27*, 1001–1011.

Narayanaswamy, P., Shinde, S., Sulc, R., Kraut, R., Staples, G., Thiam, C.H., Grimm, R., Sellergren, B., Torta, F., and Wenk, M.R. (2014). Lipidomic "deep profiling": an enhanced workflow to reveal new molecular species of signaling lipids. Anal. Chem. *86*, 3043–3047.

Nguyen, L.N., Ma, D., Shui, G., Wong, P., Cazenave-Gassiot, A., Zhang, X., Wenk, M.R., Goh, E.L.K., and Silver, D.L. (2014). Mfsd2a is a transporter for the essential omega-3 fatty acid docosahexaenoic acid. Nature *509*, 503–506.

Nguyen, T.Q., Vu, T.M., Tukijan, F., Muralidharan, S., Foo, J.C., Li Chin, J.F., Hasan, Z., Torta, F., and Nguyen, L.N. (2020). Erythrocytes efficiently utilize exogenous sphingosines for S1P synthesis and export via Mfsd2b. J. Biol. Chem. *296*, 100201.

Olivera, A., Eisner, C., Kitamura, Y., Dillahunt, S., Allende, L., Tuymetova, G., Watford, W., Meylan, F., Diesner, S.C., Li, L., et al. (2010). Sphingosine kinase 1 and sphingosine-1-phosphate receptor 2 are vital to recovery from anaphylactic shock in mice. J. Clin. Invest. *120*, 1429–1440.

Paik, J.H., Skoura, A., Chae, S.S., Cowan, A.E., Han, D.K., Proia, R.L., and Hla, T. (2004). Sphingosine 1-phosphate receptor regulation of N-cadherin mediates vascular stabilization. Genes Dev. *18*, 2392–2403.

Rosen, H., and Goetzl, E.J. (2005). Sphingosine 1-phosphate and its receptors: an autocrine and paracrine network. Nat. Rev. Immunol. *5*, 560–570.

Sato, K., Malchinkhuu, E., Horiuchi, Y., Mogi, C., Tomura, H., Tosaka, M., Yoshimoto, Y., Kuwabara, A., and Okajima, F. (2007). Critical role of ABCA1 transporter in sphingosine 1-phosphate release from astrocytes. J. Neurochem. *103*, 2610–2619.

Spiegel, S., and Milstien, S. (2011). The outs and the ins of sphingosine-1-phosphate in immunity. Nat. Rev. Immunol. *11*, 403–415.

Stenman, J.M., Rajagopal, J., Carroll, T.J., Ishibashi, M., Mcmahon, J., and Mcmahon, A.P. (2008). Canonical Wnt signaling regulates organ-specific assembly and differentiation of CNS vasculature. Science *322*, 1247–1250.

Takabe, K., Kim, R.H., Allegood, J.C., Mitra, P., Ramachandran, S., Nagahashi, M., Harikumar, K.B., Hait, N.C., Milstien, S., and Spiegel, S. (2010). Estradiol induces export of sphingosine 1-phosphate from breast cancer cells via ABCC1 and ABCG2. J. Biol. Chem. *285*, 10477–10486.

Tan, S.T., Ramesh, T., Toh, X.R., and Nguyen, L.N. (2020). Emerging roles of lysophospholipids in health and disease. Prog. Lipid Res. *80*, 101068.

Venkataraman, K., Thangada, S., Michaud, J., Oo, M.L., Ai, Y., Lee, Y.M., Wu, M., Parikh, N.S., Khan, F., Proia, R.L., and Hla, T. (2006). Extracellular export of sphingosine kinase-1a contributes to the vascular S1P gradient. Biochem. J. *397*, 461–471.

Vogt, K., Mahajan-Thakur, S., Wolf, R., Bröderdorf, S., Vogel, C., Böhm, A., Ritter, C.A., Gräler, M., Oswald, S., Greinacher, A., et al. (2018). Release of platelet-derived sphingosine-1-phosphate involves multidrug resistance protein 4 (MRP4/ABCC4) and is inhibited by statins. Thromb. Haemost. *118*, 132–142.

Vu, T.M., Ishizu, A.N., Foo, J.C., Toh, X.R., Zhang, F., Whee, D.M., Torta, F., Cazenave-Gassiot, A., Matsumura, T., Kim, S., et al. (2017). Mfsd2b is essential for the sphingosine-1-phosphate export in erythrocytes and platelets. Nature *550*, 524–528.

Wang, Y., Cho, C., Williams, J., Smallwood, P.M., Zhang, C., Junge, H.J., and Nathans, J. (2018). Interplay of the Norrin and Wnt7a/Wnt7b signaling systems in blood-brain barrier and blood-retina barrier development and maintenance. Proc. Natl. Acad. Sci. USA *115*, E11827–E11836.

Wang, Z., Zheng, Y., Wang, F., Zhong, J., Zhao, T., Xie, Q., Zhu, T., Ma, F., Tang, Q., Zhou, B., and Zhu, J. (2020). Mfsd2a and Spns2 are essential for sphingosine-1-phosphate transport in the formation and maintenance of the blood-brain barrier. Sci. Adv. *6*, eaay8627.

Wong, B.H., Chan, J.P., Cazenave-Gassiot, A., Poh, R.W., Foo, J.C., Galam, D.L.A., Ghosh, S., Nguyen, L.N., Barathi, V.A., Yeo, S.W., et al. (2016). Mfsd2a is a transporter for the essential omega-3 fatty acid docosahexaenoic acid (DHA) in eye and is important for photoreceptor cell development. J. Biol. Chem. *291*, 10501–10514.

Yanagida, K., and Hla, T. (2017). Vascular and immunobiology of the circulatory sphingosine 1-phosphate gradient. Annu. Rev. Physiol. *79*, 67–91.

Yanagida, K., Engelbrecht, E., Niaudet, C., Jung, B., Gaengel, K., Holton, K., Swendeman, S., Liu, C.H., Levesque, M.V., Kuo, A., et al. (2020). Sphingosine 1-phosphate receptor signaling establishes AP-1 gradients to allow for retinal endothelial cell specialization. Dev. Cell *52*, 779–793.e7.

Yanagida, K., Liu, C.H., Faraco, G., Galvani, S., Smith, H.K., Burg, N., Anrather, J., Sanchez, T., Iadecola, C., and Hla, T. (2017). Size-selective opening of the blood-brain barrier by targeting endothelial sphingosine 1-phosphate receptor 1. Proc. Natl. Acad. Sci. USA *114*, 4531–4536.

Zhou, Y., and Nathans, J. (2014). Gpr124 controls CNS angiogenesis and blood-brain barrier integrity by promoting ligand-specific canonical wnt signaling. Dev. Cell *31*, 248–256.

Zhou, Y., Wang, Y., Tischfield, M., Williams, J., Smallwood, P.M., Rattner, A., Taketo, M.M., and Nathans, J. (2014). Canonical WNT signaling components in vascular development and barrier formation. J. Clin. Invest. *124*, 3825–3846.

STAR★METHODS

KEY RESOURCES TABLE

REAGENT or RESOURCE	SOURCE	IDENTIFIER
Antibodies		
Mouse Alexa Fluor 488-conjugated Claudin 5	ThermoFisher Scientific	Cat# 352588; RRID: N/A
Mouse CD140B (PDGFRB)	Life Technologies	Cat# 14-1402-82; RRID: AB_467493
Mouse Glut1	Abcam	Cat# ab40084; RRID: AB_2190927
Rabbit Non-phospho (active) beta-Catenin (Ser45) (D2U8Y)	Cell Signaling Technology	Cat# 19807; RRID: AB_2650576
Rabbit Phospho beta-Catenin (Ser33/37/Thr41)	Cell Signaling Technology	Cat# 9561; RRID: AB_331729
Purified Rat Anti Mouse CD31	BD Pharmingen	Cat# 553370; RRID: AB_394816
Purified Rat Anti-Mouse Ter119/Erythroid Cells	BD Pharmingen	Cat# 553670; RRID: AB_394983
Rabbit Phosphorylated Smad4 (D3M6U)	Cell Signaling Technology	Cat# 38454; RRID: AB_2728776
Rat CD144 (VE-cadherin)	Invitrogen by Thermo Fisher Scientific	Cat# 14-1441-82; RRID: AB_842767
Rabbit Phospho-p44/42 MAPK (Erk1/2)	Cell Signaling Technology	Cat# 4370S; RRID: AB_2315112
Rabbit p44/42 MAPK (Erk1/2)	Cell Signaling Technology	Cat# 9102S; RRID: AB_330744
Purified Rat Anti-Mouse Panendothelial Cell Antigen (PLVAP)	BD Pharmingen	Cat# 553849; RRID: N/A
Mouse N-cadherin	Invitrogen	Cat# 33-3900; RRID: AB_2313779
Mouse Anti-Actin, α-Smooth Muscle - Cy3™	Sigma-Aldrich	Cat# C6198; RRID: AB_476856
Mouse Anti-GAPDH	Santa Cruz	Cat# sc-32233; RRID: AB_627679
Mouse Alexa Fluor 488-conjugated Occludin	ThermoFisher Scientific	Cat# 331588; RRID: AB_2532185
Mouse anti-beta-actin	Sigma-Aldrich	Cat# A5441; RRID: AB_476744
Rabbit anti-Ki67	Abcam	Cat# ab15580; RRID: AB_443209
Rabbit anti-ERG	Abcam	Cat# ab92513; RRID: AB_2630401
Mouse CD31 Monoclonal antibody (WM59)	Invitrogen	MA1-26196
Alexa Fluor 488 goat Anti-Rat	Invitrogen by Thermo Fisher Scientific	Cat# A11006; RRID: AB_2534074
Alexa Fluor 555 goat Anti-Rat	Invitrogen by Thermo Fisher Scientific	Cat# A21434; RRID: AB_2535855
Alexa Fluor Plus 488 donkey anti-Mouse IgG (H + L)	Invitrogen by Thermo Fisher Scientific	Cat# A32766; RRID: AB_2762823
IRDye® 800CW Donkey anti-Mouse IgG	LI-COR Biosciences	Cat# 926-32212; RRID: AB_621847
IRDye® 800CW Donkey anti-Rabbit IgG	LI-COR Biosciences	Cat# 926-32213; RRID: AB_621848
IRDye® 800CW Donkey anti-Goat IgG	LI-COR Biosciences	Cat# 926-32214; RRID: AB_621846
IRDye® 680LT Goat anti-Mouse IgG Secondary Antibody	LI-COR Biosciences	Cat# 925-68020; RRID: AB_2687826
IRDye® 680RD Donkey anti-Rabbit IgG Secondary Antibody	LI-COR Biosciences	Cat# 926-68073; RRID; AB_10954442
*InVivo*Plus anti-mouse Ly6G/Ly6C (Gr-1)	BXcell, clone RB6-8C5	Cat# BP0075; RRID: AB_10312146
Deposited data		
Raw lipidomic data	This manuscript	Mendeley Data: https://doi.org/10.17632/ypbs67rtsh.1 RRID: N/A
Chemicals, peptides, and recombinant proteins		
polyIC	InvivoGen	tlrl-pic-5
Sphingosine (D-erythro-sphingosine)	Avanti	Cat# 860490 RRID: 860490P-25MG
Sphingosine-1-phosphate (D-erythro-sphingosine-1-phosphate)	Avanti	Cat# 860492 RRID: 860492P-1MG

(*Continued on next page*)

Continued

REAGENT or RESOURCE	SOURCE	IDENTIFIER
Fatty acid-free bovine serum albumin (BSA)	Sigma	Cat# A7030 RRID: N/A
Histamine	Sigma	Cat# H7125 RRID: H7125-1G
Sulfo-NHS-biotin	Thermo Fisher	Cat# 21217 RRID: N/A
EDTA-K2	Sigma Aldrich	Cat# ED2P RRID: ED2P-100G
Paraformaldehide	Sigma Aldrich	Cat# 441244 RRID: 441244-1KG
Tyrode-H buffer (10 mM HEPES-NaOH, 12 mM $NaHCO_3$, 138 mM NaCl, 5.5 mM D-glucose, 2.9 mM KCl, 1 mM $MgCl_2$, pH 7.4)	This manuscript	RRID: N/A
[3-^{3}H] sphingosine	American Radiolabeled Chemicals, Inc.	ART 0490 RRID: N/A
RIPA buffer (25mM Tris pH 7.4, 150 mM NaCl, 0.1% SDS, 0.5% sodium deoxycholate, 0.5% Triton X-100)	This manuscript	RRID: N/A
Protease inhibitor cocktail	Roche	Cat# 11836170001 RRID: N/A
Protease inhibitor and phosphatase inhibitor cocktail 1	Sigma-Aldrich	Cat# P2850 RRID: N/A
RNeasy Mini kit	Qiagen	Cat# 74104 RRID: N/A
SuperScript III First strand synthesis kit	ThermoFisher	Cat# 18080051 RRID: N/A
SYBR Green Master Mix	Bio-Rad Laboratories	Cat# 1725271 RRID: N/A
Streptavidin-Texas red	Vector Laboratory	Cat#SA-5006 RRID: N/A
Xylene	Sigma Aldrich	Cat# 1330-20-7 RRID: N/A
Haematoxylin	Merck	Cat# 1.05174.2500 RRID: N/A
Eosin	Sigma Aldrich	Cat# HT110380 RRID: N/A
DPX mountant	Merck	Cat# 06522 RRID: N/A
Evans Blue	Sigma Aldrich	Cat# 314-13-6 RRID: N/A
Formamide	Sigma Aldrich	Cat# 75-12-7 RRID: N/A
SEW2871	Cayman Chemical	Cat# 10006440 RRID: N/A
DMSO	Sigma Aldrich	Cat#D8418 RRID: D8418-250ML
Tween-20	Sigma Aldrich	Cat# P1379 RRID: P1379-500ML
Critical commercial assays		
Biovision Histamine (HIS) Elisa kit	BioVision	Cat# K4163-100 RRID: N/A
Experimental models: Organisms/strains		
C57BL/6-Mfsd2b$^{tm1a(KOMP)Wtsi}$	KOMP	IMPC: https://www.mousephenotype.org/data/genes/MGI:3583946 RRID: N/A
C57BL/6-Spns2$^{tm1a(KOMP)Wtsi}$	KOMP	IMPC: https://www.mousephenotype.org/data/genes/MGI:2384936 RRID: N/A
Mfsd2b$^{f/f}$	This manuscript	RRID: N/A
Spns2$^{f/f}$	This manuscript	RRID: N/A
Mfsd2b$^{-/-}$;Spns2$^{+/-}$	This manuscript	RRID: N/A
Spns2$^{f/f}$ Mfsd2b$^{f/f}$	This manuscript	RRID: N/A
Sphk1$^{f/f}$:Sphk2$^{-/-}$	This manuscript	RRID: N/A
Sphk1$^{-/-}$:Sphk2$^{f/f}$	This manuscript	RRID: N/A
Oligonucleotides		
See Table S2 for qPCR primers		
Software and algorithms		
GraphPrism9	GraphPad software	http://www.graphpad.com RRID: SCR_002798
ImageJ	Software	https://imagej.nih.gov/ij/ RRID: SCR_003070

(*Continued on next page*)

Continued

REAGENT or RESOURCE	SOURCE	IDENTIFIER
ImageLab	Software	https://www.bio-rad.com/en-au/product/image-lab-software RRID: N/A
MassHunter Quantitative Analysis (QQQ)	Software	RRID: N/A
Others		
Celltex-α MEK-6400	Nihon Kohden	RRID: N/A
Tri-carb	GE Healthcare	RRID: N/A
ChemiDocMP	Bio-rads	RRID: N/A
Rectal thermometer	RET-3, Type J/K/T Thermocouple Thermometer	RRID: N/A
Tail cup methods	Visitech System, USA	Cat# BP2000 RRID: N/A

RESOURCE AVAILABILITY

Lead contact

Further information and requests for resources and reagents should be directed to and will be fulfilled by the lead contact, Dr. Long N. Nguyen (bchnnl@nus.edu.sg).

Materials availability

All unique/stable reagents generated in this study are available from the lead contact with a completed materials transfer agreement if required. Please note that there are restrictions to the availability of the double knockout mice generated in this study due to lack of centralized repository. Thus, the single knockout mice might be available upon request to the lead contact.

Data and code availability

- Raw lipidomic data have been deposited at Mendeley Data website and are publicly available as of the date of publication. Accession numbers are listed in the key resources table. All data reported in this paper will be shared by the lead contact upon request.
- This paper does not report original code.
- Any additional information required to reanalyze the data reported in this paper is available from the lead contact upon request.

EXPERIMENTAL MODEL AND SUBJECT DETAILS

Mice

Global knockout mice of *Mfsd2b* were generated from frozen sperm obtained from KOMP (Vu et al., 2017). *Spns2* knockout mice were obtained from KOMP. All mice were in C57BL/6 background. Double global knockout ($Mfsd2b^{-/-}$;$Spns2^{-/-}$, hereafter gDKO) embryos were generated by inter-crossing $Mfsd2b^{-/-}$;$Spns2^{+/-}$ mice. Timed-mating was conducted using female mice with 3–6 months old; and pregnant $Mfsd2b^{-/-}$;$Spns2^{+/-}$ females were dissected at 12.5, 13.5, 14.5, and 15.5 days post-coitum to collect the fetuses. The gender of embryos was not determined. Double global knockout and control embryos ($Mfsd2b^{-/-}$;$Spns2^{+/-}$ or $Mfsd2b^{-/-}$;$Spns2^{+/+}$) were used. Double conditional knockout mice for *Mfsd2b*&*Spns2* were generated by inter-crossing homozygous floxed *Mfsd2b* ($Mfsd2b^{f/f}$) Spns2 ($Spns2^{f/f}$) mice with $Spns2^{f/f}$ $Mfsd2b^{f/f}$ mice containing Mx1Cre. Deletion of both *Mfsd2b* and *Spns2* was induced by polyIC. Three consecutive doses of polyIC (100μg/pub) were injected to intraperitoneal of P5 to P7 pups (P5-7). Compound conditional knockout $Mfsd2b^{f/f}$;$Spns2^{f/f}$;Mx1Cre (hereafter, ctDKO-Mx1Cre) with WBC of $<2.5x10^3/\mu l$ and control mice aged >3–12 months old ($Mfsd2b^{f/f}$;$Spns2^{f/f}$) were used for experiments. Deletion of *Mfsd2b* in red blood cells (RBC) was confirmed by S1P transport activity and Western blot, while deletion of *Spns2* was confirmed by enumerating white blood cells (WBCs). Double conditional knockout mice for Sphk1&SphK2 (ckDKO-Mx1Cre) were generated by crossing $Sphk1^{f/f}$:$Sphk2^{-/-}$:Mx1Cre males to $Sphk1^{-/-}$:$Sphk2^{f/f}$ females and by induction of pups with polyIC postnatally as previously described (Gazit et al., 2016). Mice were maintained at a constant temperature of 20°C with 12-h light/12-h dark cycle on normal chow diets. All experimental protocols and procedures in the protocol R19-0567 were approved by IACUC committees under National University of Singapore.

METHOD DETAILS

Chemicals

Sphingosine (D-erythro-sphingosine, 860490P-25MG), sphingosine-1-phosphate (D-erythro-sphingosine-1-phosphate, 860492P-1MG) were purchased from Avanti. Fatty acid-free bovine serum albumin (BSA) and histamine were purchased from Sigma (Cat.

A7030-100G). PolyIC was purchased from Invitrogen (Cat. tlrl-pic-5). Sulfo-NHS-biotin was purchased from Thermo Fisher (Cat. 21217).

Antibodies

The rabbit polyclonal antibody for *Mfsd2b* was generated as described previously (Vu et al., 2017) and used at 1:500 for Western blot. Gapdh was used as an endogenous control. Other primary antibodies and secondary antibodies used for immunofluorescent staining and Western blot are listed in Table S2.

Complete blood count

Blood was collected into EDTA-K2-coated tubes by heparinized capillary and directly counted using Celltex-α MEK-6400 (Nihon Kohden). Blood collected for WBC count was performed between 10am-12pm.

Quantitative PCR

Fetal livers from pure WT, Mfsd2b$^{-/-}$ and gDKO were collected for RNA extraction using RNeasy Mini kit (Qiagen, Cat. 74104). cDNA was synthesized using SuperScript III First strand synthesis kit (ThermoFisher, Cat. 18080051). Quantitative PCR reaction was conducted using SYBR Green Master Mix (BioRaq, Cat. 1725271) to examine *Mfsd2b* and *Spns2* expression at mRNA level. The in-house designed primers were listed in Table S2. The fold change was analyzed using 2–ΔΔCt method.

Immunohistochemistry

Embryos were removed from the mother and fixed in 4% paraformaldehyde in PBS at 4°C overnight. They were then preserved in 30% sucrose (in water) for cryo-sectioning. Coronal cryo-sections of 30μm thickness from fetuses were prepared for immunohistochemistry with the following primary antibodies: anti-Glut1 (Abcam, Cat. ab40084), anti-Ter119 (BD pharmingen, Cat. 553670), anti-CD31(BD pharmingen, Cat. 553370), anti-CD144 (VE-Cadherin) (Invitrogen, Cat. 14-1441-82), anti-Claudin-5 (ThermoFisher Scientific, Cat. 352588); PDGFRβ (Life Technologies, Cat. 14-1402-82); PLVAP (BD Pharmingen, Cat. 553849); anti-N-cadherin (Invitrogen, Cat. 33-3900), anti-α-Smooth Muscle actin-Cy3^{TM} (Sigma-Aldrich, Cat. C6918), anti-Ki67 (Abcam, Cat. ab15580), and anti-ERG (Abcam, Cat. ab92513). Secondary antibodies used for detection included: AF488- (Invitrogen, Cat. A11006) and AF555- (Invitrogen, Cat. A21434). Sections were counterstained with 4,6-diamidino-2-phenylindole (DAPI) for cell nuclei visualization. Specimens were imaged with a confocal microscope (LSM710, Carl Zeiss) using 10×, 20× and 63× objectives.

Transport assay with red blood cells

Blood was collected into 5% EDTA-K2 tubes and washed immediately twice with Tyrode-H buffer (10 mM HEPES-NaOH, 12 mM $NaHCO_3$, 138 mM NaCl, 5.5 mM D-glucose, 2.9 mM KCl, 1 mM $MgCl_2$, pH 7.4). For transport assays, 20 million erythrocytes (RBCs) were incubated with 2 μM [3-^{3}H] sphingosine in 200 μL Tyrode-H buffer containing 0.5% BSA for 30 min at 37°C. Then, cell pellets (RBCs) and supernatants were separated by centrifugation at 1500 rpm for 5 min at room temperature. Cell pellets were washed once with 500 μL Tyrode-H buffer containing 0.5% BSA. Cell pellets and supernatant were subjected to S1P isolation using alkaline extraction. For radioactive counting, the same amount of aqueous phase containing S1P was mixed with scintillant (MP Biomedicals) and quantified using Tri-carb (GE Healthcare).

Similar transport assays were also performed with primitive RBC and fetal liver cells from Mfsd2b$^{-/-}$ and Spns2$^{-/-}$ embryos and control embryos. For primitive RBC collection, E17.5 and E18.5 embryos were bled into warm PBS. Primitive RBCs were collected for transport assays as described above for mature RBC. Fetal livers from E17.5 and E18.5 embryos were also harvested and minced by a syringe plunger. The fetal liver cells were then passed through 75μm cell strainers before harvesting for transport assays. Transport activity of primitive RBC from Mfsd2b$^{-/-}$ or Spns2$^{-/-}$ embryos were normalized to that of control littermates (WT and heterozygous embryos).

In vivo transport assay with [3-^{3}H] sphingosine

Mice were intravenously injected with [3-^{3}H] sphingosine solubilized in 12% BSA (Dose: 1μL of 1 mM [3-^{3}H] sphingosine/gram body weight; specific activity: 10 μCi/mL). One minute later, 10μL blood was collected to monitor the initial signals. Blood samples were collected at 10, 30, 60, 120, and 180 min. Blood cells were spun down to collect plasma and RBCs. To harvest the remaining plasma, the cell pellets were washed once with Tyrode-H containing 0.1% BSA and spun down to collect the supernatant. The supernatant was combined with the plasma. The cell pellets and supernatant samples were subjected to S1P isolation by alkaline extraction. The radioactive signals of S1P from different time points were normalized to the S1P signal from WT collected at 10 min.

Western blot analysis

Washed RBCs were lysed in RIPA buffer (25mM Tris pH 7.4, 150 mM NaCl, 0.1% SDS, 0.5% sodium deoxycholate, 0.5% Triton X-100) supplemented with protease inhibitor cocktail (Roche, 11836170001). An amount of 150 μg protein lysates was resolved on 10% SDS-PAGE, and transferred to nitrocellulose membrane. Brains were freshly harvested from E13.5 embryos and lysed with RIPA buffer supplemented with protease inhibitor and phosphatase inhibitor cocktail 1 (Sigma-Aldrich, P2850). An amount of 75μg whole brain lysates was similarly utilized for Western blot analysis. Lung tissues perfused with PBS after histamine challenging

(10mg/kg BW) were collected and lysed with RIPA buffer supplemented with protease inhibitor and phosphatase inhibitor cocktail 1 (Sigma-Aldrich, P2850). An equal amount of 50μg total protein of lung lysates was used for Western blot analysis. Primary and secondary antibodies for detection are listed in Table S2. ChemiDocMP (Bio-rads) system was used for detection. The protein bands were quantified by ImageLab software.

Plasma collection for lipidomic analysis

Blood was collected under isoflurane anesthesia into EDTA-K2 collection tubes from the retro-orbital venous plexus with heparin-collected capillaries. Plasma was collected from blood samples after centrifugation at 2500 rpm for 30 min at room temperature. Blood samples with signs of hemolysis were excluded. Plasma was kept at −80°C until further analysis.

Lipidomics

S1P analysis was performed using LC-MS/MS mass spectrometer as described previously (Narayanaswamy et al., 2014), (Chandrakanthan et al., 2021). Plasma samples from control and knockout mice aged 1-month and 4-months old were analyzed. For S1P analysis, plasma samples were first spiked with an internal standard (13C22H2-S1P, Toronto Chemicals), lipid extraction using a 1-butanol/methanol (1:1) mixture, followed by derivatisation with TMS-diazomethane. LC-MS/MS was performed on a UHPLC 1290 Agilent liquid chromatograph connected to a 6495A Triple Quadrupole mass spectrometer. Peak integration was performed using MassHunter Quantitative Analysis (QQQ) software, and data were manually curated to ensure correct peak integration. Areas under the curve (AUC) were corrected for isotopic interference where needed (Gao et al., 2021). One-point calibration was used to calculate the molar concentrations of the lipids. The stability of signal throughout the analysis was monitored by regular injection of a quality control samples. The levels of individual S1P were quantified and normalized to internal standards. Total levels of S1P were calculated and expressed as indicated in the figures.

Body temperature measurements

Histamine (1mg/25g body weight) prepared in PBS was injected via retro-orbital vein to aged-match WT and ctDKO-Mx1Cre mice. Core body temperature of WT and ctDKO-Mx1Cre mice was recorded using a rectal probe with thermometer (RET-3, Type J/K/T Thermocouple Thermometer). Core body temperature was recorded every 5 min for a duration of 60 min after histamine injection. For rescue experiments, a bolus of S1P (18:1) in 12% BSA was i.v. injected to achieve final concentration of 500μM in blood. Injection volume was kept at 100μL for S1P and vehicle (12% BSA in PBS).

Blood pressure measurements

Basal blood pressure was measured in both male WT and ctDKO-Mx1Cre mice aged 3–4 months using tail cup methods (BP2000, Visitech System, USA). Systolic blood pressure BP was monitored before histamine injection. For histamine-induced hypotension, histamine (0.25mg/25g BW) was injected via retro-orbital vein and systolic blood pressure was recorded 45, 60, and 90 min after histamine challenge. Six measurement cycles/each time point were collected and averaged.

Histamine clearance

To determine the histamine clearance in plasma, histamine (1mg/25g BW) was intravenously injected to male ctDKO-Mx1Cre and control mice aged 3–4 months old. Blood was drawn at 25 and 60 min for plasma collection by centrifugation at 2500rpm as described above. Histamine levels were measured by ELISA according to vendor description (Bio Vison Histamine (HIS) Elisa kit; Cat. K4163-100).

Sulfo-NHS-biotin extravasation

WT and ctDKO-Mx1Cre mice were intravenously injected with histamine (1mg/25g BW). After 10 min, a bolus of Sulfo-NHS-Biotin (0.5mg/g body weight) was intravenously injected. Ten minutes later, mice were transcardially perfused with 10mL PBS for 5 min and the brain was fixed with 4% PFA for dissection. To detect biotin extravasation, the brain was transferred carefully into 5mL-tube and incubated with Texas Red®Strepavidin diluted in PBS +0.5% Triton X-100 + 0.1 mM $CaCl_2$ with 10% normal goat serum at 4°C overnight. Images were acquired on confocal microscope (LSM710, Carl Zeiss) using 10×, 20× and 63× objectives (Wong et al., 2016), (Zhou and Nathans, 2014).

Paraffin sections

For histological assessments, lungs were collected from 3-4 months old control and ctDKO-Mx1Cre mice 25 min after histamine challenge (1mg/25g BW, i.v. route). Lungs were immediately inflated with 1% PFA and fixed with 4% PFA for dissections. Paraffin sections from embryos were similarly prepared. For H&E staining, after dehydration using 70–100% ethanol followed by xylene (Sigma Aldrich, Germany, Cat. 1330-20-7), lung tissues or embryos were embedded in paraffin and then dissected using a microtome. The slides were tipped in xylene chamber to remove paraffin. Then, the slides were rehydrated progressively with 100 to 70% ethanol for 10 min each and rinsed with tap water for 5 min. The sections were stained with haematoxylin (Merck, Germany, Cat. 1.05174.2500) for 2 min and washed with tap water until excessed stain is thoroughly removed. Slides were tipped with 95% ethanol to dehydrate and then stained for 2 min with eosin (Sigma Aldrich, USA, Cat. HT110380). The excessed dyes were removed

by washing with 50 to 100% ethanol in 2 min interval and the slides were cleared with xylene (Sigma Aldrich, Germany, Cat. 1330-20-7) for 5 min. The slides were air-dried and covered by DPX mountant (Merck, Germany, Cat. 06522) for imaging.

Myeloid cell depletion

Control and ctDKO-Mx1Cre mice were injected via peritoneal with 500μg Ly6C/Ly6G antibody (BXcell, clone RB6-8C5, cat: BP0075). Ly6C/Ly6G antibody treatment depletes both monocytes and neutrophils. Complete blood cells were enumerated before and 40 h after the antibody treatment. Plasma samples at these time points were also collected for S1P analysis as described above. Similarly, mice with myeloid depletion were also assessed for Evans Blue leakage. Control and ctDKO-Mx1Cre mice 40 h post-treatment with Ly6C/Ly6G antibody were injected with 100μL of 1.5% Evans Blue in PBS (Sigma Aldrich, Germany, Cat. 314-13-6). The mice were perfused with 20 mL PBS for 5 min and lungs were harvested for quantification of Evans Blue accumulation.

Evans blue extravasation

Control and ctDKO-Mx1Cre mice were injected with 100μL of 1.5% Evans Blue solution prepared in PBS through retro-orbital vein to assess vascular leakages in the lungs and brains. After 30 min, mice were anesthetized using ketamine solution (100 μL/10g BW, i.p. route) following by a perfusion with PBS solution. The lungs and brains were removed, photographed, and dried at 60°C overnight. To extract Evans Blue, dried lung and brain samples were immerged in 1 mL formamide solution (Sigma Aldrich, Germany, Cat. 75-12-7) for 4 days at room temperature. Evans Blue dye extract was determined as the absorbance of OD_{620} subtracted OD_{500}.

Drug treatment

To assess whether SEW2871, a S1PR1 agonist, could rescue the lung vascular leakage phenotype, control and ctDKO-Mx1Cre mice (six to seven mice per group) were first injected i.p. with a 20 mg/kg of SEW2871 or saline that was dissolved in 10% DMSO and 25% Tween-20 as vehicle. 30 min later, the mice were i.v injected with 100μL of 1.5% Evans Blue solution prepared in PBS through retro-orbital vein to assess vascular leakages in the lungs and brains. After 30 min, mice were anesthetized using ketamine solution (100 μL/10g BW, i.p. route) following by a perfusion with PBS solution. The lungs and brains were removed, photographed, and dried at 60°C overnight. To extract Evans Blue, dried lung and brain samples were immerged in 1 mL formamide solution (Sigma Aldrich, Germany, Cat. 75-12-7) for 4 days at room temperature. Evans Blue dye extract was determined as the absorbance of OD_{620} subtracted OD_{500}.

To examine the low level of plasma S1P in ckDKO-Mx1Cre, Mx1 Sphk1f/-:2f/- females and littermate controls were treated with 10 mg/L DOP, an inhibitor for S1P lyase SGPL1 in drinking water supplied with 10g/L sucrose. Plasma and complete blood cell count were performed before and 3 days post DOP treatment. Plasma S1P was analyzed as described above.

Irradiation

4–5 months old controls, ctDKO-Mx1Cre, and ckDKO-Mx1Cre mice were irradiated with a single dose of 6.5Gy. Plasma from the mice were collected before and 6 days post-irradiation for S1P analysis.

QUANTIFICATION AND STATISTICAL ANALYSIS

Quantification of immunostaining

Immunofluorescence intensity of VE-Cadherin and Claudin-5 was quantified by ImageJ. The intensity values of VE-Cadherin and Claudin-5 staining in blood vessels were quantified and normalized to background signals in each area. $Ki67^+$ and ERG^+ cells were quantified by ImageJ using cell count function. Number of $Ki67^+$ cells was displayed as ratio of total $Ki67^+$cells/total number of cells in each aorta. Number of ERG^+ cells was displayed as ratio of total ERG^+ cells/total $CD31^+$ cells in each aorta.

Blood vessel density

To quantify the vascular density and width, CNS blood vessels were stained with CD31 or Glut1. The vascular density in midbrain, ganglionic eminences was quantified by ImageJ and expressed as percentage of measured areas. The diameter of blood vessels was also quantified by ImageJ. To quantify diameters of blood vessels, CNS vasculature was stained with Glut1 and peripheral vasculature was stained with CD31 for visualization. Images were taken with a confocal microscope at 63× objective. The biggest blood vessels (usually 5–10 blood vessels) in each image were chosen for measuring their diameters followed by instructions from ImageJ software.

Statistical analysis

Data were analyzed using GraphPrism9 software. For parametric data, t test, one-way ANOVA, or two-way ANOVA was used for calculation of p values. For non-parametric data, Mann-Whitney U or Kruskal-Wallis test were used for calculation of p values. p value <0.05 was considered as statistically significant.